

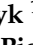




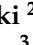



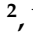

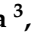




## Article

# The Effect of Fluorides (BaF<sub>2</sub>, MgF<sub>2</sub>, AlF<sub>3</sub>) on Structural and Luminescent Properties of Er<sup>3+</sup>-Doped Gallo-Germanate Glass

Magdalena Leśniak <sup>1,\*</sup>, Gabriela Mach <sup>1</sup>, Bartłomiej Starzyk <sup>1</sup>, Karolina Sadowska <sup>2</sup>, Tomasz Ragiń <sup>2</sup>, Jacek Żmojda <sup>2</sup>, Marcin Kochanowicz <sup>2</sup>, Marta Kuwik <sup>3</sup>, Piotr Miluski <sup>2</sup>, Gloria Lesly Jimenez <sup>1</sup>, Agata Baranowska <sup>4</sup>, Jan Dorosz <sup>2</sup>, Wojciech Pisarski <sup>3</sup>, Joanna Pisarska <sup>3</sup>, Zbigniew Olejniczak <sup>5</sup> and Dominik Dorosz <sup>1</sup>

- <sup>1</sup> Faculty of Materials Science and Ceramics, AGH University of Science and Technology, 30 Mickiewicza Av., 30-059 Krakow, Poland; machgabriela1@gmail.com (G.M.); starzyk@agh.edu.pl (B.S.); glesly@agh.edu.pl (G.L.J.); ddorosz@agh.edu.pl (D.D.)
  - <sup>2</sup> Faculty of Electrical Engineering, Bialystok University of Technology, 45D Wiejska Street, 15-351 Bialystok, Poland; k.sadowska@doktoranci.pb.edu.pl (K.S.); tomasz.ragin@pb.edu.pl (T.R.); j.zmojda@pb.edu.pl (J.Ż.); m.kochanowicz@pb.edu.pl (M.K.); p.miluski@pb.edu.pl (P.M.); doroszjan@pb.edu.pl (J.D.)
  - <sup>3</sup> Institute of Chemistry, University of Silesia, 9 Szkolna Street, 40-007 Katowice, Poland; marta.kuwik@ud.edu.pl (M.K.); wojciech.pisarski@us.edu.pl (W.P.); joanna.pisarska@us.edu.pl (J.P.)
  - <sup>4</sup> Faculty of Mechanical Engineering, Bialystok University of Technology, 45C Wiejska Street, 15-351 Bialystok, Poland; a.baranowska@pb.edu.pl
  - <sup>5</sup> Institute of Nuclear Physics, Polish Academy of Sciences, Radzikowskiego 152, 31-342 Krakow, Poland; zbigniew.olejniczak@ifj.edu.pl
- \* Correspondence: mlesniak@agh.edu.pl



**Citation:** Leśniak, M.; Mach, G.; Starzyk, B.; Sadowska, K.; Ragiń, T.; Żmojda, J.; Kochanowicz, M.; Kuwik, M.; Miluski, P.; Jimenez, G.L.; et al. The Effect of Fluorides (BaF<sub>2</sub>, MgF<sub>2</sub>, AlF<sub>3</sub>) on Structural and Luminescent Properties of Er<sup>3+</sup>-Doped Gallo-Germanate Glass. *Materials* **2022**, *15*, 5230. <https://doi.org/10.3390/ma15155230>

Academic Editor: Alessandra Toncelli

Received: 20 June 2022

Accepted: 23 July 2022

Published: 28 July 2022

**Publisher's Note:** MDPI stays neutral with regard to jurisdictional claims in published maps and institutional affiliations.



**Copyright:** © 2022 by the authors. Licensee MDPI, Basel, Switzerland. This article is an open access article distributed under the terms and conditions of the Creative Commons Attribution (CC BY) license (<https://creativecommons.org/licenses/by/4.0/>).

**Abstract:** The effect of BaF<sub>2</sub>, MgF<sub>2</sub>, and AlF<sub>3</sub> on the structural and luminescent properties of gallo-germanate glass (BGG) doped with erbium ions was investigated. A detailed analysis of infrared and Raman spectra shows that the local environment of erbium ions in the glass was influenced mainly by [GeO]<sub>4</sub> and [GeO]<sub>6</sub> units. Moreover, the highest number of non-bridging oxygens was found in the network of the BGG glass modified by MgF<sub>2</sub>. The <sup>27</sup>Al MAS NMR spectrum of BGG glass with AlF<sub>3</sub> suggests the presence of aluminum in tetra-, penta-, and octahedral coordination geometry. Therefore, the probability of the <sup>4</sup>I<sub>13/2</sub> → <sup>4</sup>I<sub>15/2</sub> transition of Er<sup>3+</sup> ions increases in the BGG + MgF<sub>2</sub> glass system. On the other hand, the luminescence spectra showed that the fluoride modifiers lead to an enhancement in the emission of each analyzed transition when different excitation sources are employed (808 nm and 980 nm). The analysis of energy transfer mechanisms shows that the fluoride compounds promote the emission intensity in different channels. These results represent a strong base for designing glasses with unique luminescent properties.

**Keywords:** heavy metal oxide glasses; gallo-germanate glass; BaF<sub>2</sub>; MgF<sub>2</sub>; AlF<sub>3</sub>; DSC; thermal stability; structure; IR; Raman; <sup>27</sup>Al MAS NMR spectrum; luminescence properties; erbium ions; wide emission

## 1. Introduction

One of the most popular techniques for designing glass for photonic applications is the modification of their structural properties. This is more significant in luminescent materials because the quantum efficiency of active dopants has a strong dependence on the chemical bonding type. In the past, several studies on oxide gallo-germanate glasses have been reported due to their potential use in photonics. The properties of this kind of glass have been explored in Ga<sub>2</sub>O<sub>3</sub>–GeO<sub>2</sub>–BaO [1], Ga<sub>2</sub>O<sub>3</sub>–GeO<sub>2</sub>–BaO–K<sub>2</sub>O [2], Ga<sub>2</sub>O<sub>3</sub>–GeO<sub>2</sub>–La<sub>2</sub>O<sub>3</sub>–BaO [3,4], and Ga<sub>2</sub>O<sub>3</sub>–GeO<sub>2</sub>–BaO–La<sub>2</sub>O<sub>3</sub>–Y<sub>2</sub>O<sub>3</sub> [5] systems, demonstrating that gallo-germanate glasses offer wide optical transparency (~6 μm), low phonon

energy ( $\sim 850\text{ cm}^{-1}$ ), and a high linear and nonlinear refractive index [6]. Moreover, gallo-germanate glasses are mechanically resistant and chemically stable, which allows their use in the production of fibers and waveguides [7–9].

It is well known that the presence of fluoride compounds in oxy-fluoride gallo-germanate glasses doped with rare earth ions (RE ions) affects the spectroscopic properties of the glass, due to the chemical affinity between the dopants (RE ions) and ligands (fluorides). However, their presence in the oxide glass network reduces the phonon energy, decreases non-radiative decay, and increases the emission intensity, triggering higher quantum efficiencies. On the other hand, their effect on the luminescent properties of gallo-germanate glass (BGG) doped with RE ions has been focused on the use of barium difluoride ( $\text{BaF}_2$ ); it has been found that its presence can modify the glass composition, which impacts the efficiency of the emission, optical transmission, and spectra profile [10–13].

Among the lanthanides, erbium is the most intensively studied element in luminescence because of its wide range of applications as an optical fiber amplifier, NIR fiber laser [14,15], optical temperature sensor [16], non-linear optical device [17], and up-conversion luminescent source [18] due to its unique properties. One of the most attractive applications is its use as an EDFA amplifier working in the III telecommunication window, due to its emission at 1550 nm originating from the  $^4\text{I}_{13/2} \rightarrow ^4\text{I}_{15/2}$  transition; however, its low solubility and the high-phonon energy of silicon glasses as a matrix limit the optical gain and spectral width of the amplification band [19]. For this reason, the interest in the development of new soft glasses that are able to accept a higher erbium concentration, characterized by a broadband emission in the near-infrared range (NIR), has grown [20,21], and it has been found that the use of gallo-germanate glass with  $\text{BaF}_2$  showed an increase in the linewidth at 1.55  $\mu\text{m}$  from 50 nm to 67 nm [22].

Additionally, its ability to convert near-infrared light into green and red light as a result of the up-conversion (UC) processes increases its interest [23]. In this case, if the population of higher energy states mainly occurs by the excited state absorption (ESA) and the energy transfer with up-conversion (ETU), then the green and red emission bands will be a trigger. The quantum efficiency of these transitions strictly depends on the structural properties of the host and is higher when the phonon energy is lower [24,25].

In this work, we focus on the role of different fluoride compounds ( $\text{BaF}_2$ ,  $\text{MgF}_2$ ,  $\text{AlF}_3$ ) in the structural properties of gallo-germanate glass and analyzed for a possible correlation of these features with the intensity of radiative transitions in erbium ions. For a better understanding of the energy transfer mechanism, we used the two main excitation schemes of  $\text{Er}^{3+}$  ions (800 and 980 nm), which corresponds to the  $^4\text{I}_{15/2} \rightarrow ^4\text{I}_{9/2}$  and  $^4\text{I}_{15/2} \rightarrow ^4\text{I}_{11/2}$  transitions, respectively. Moreover, we have investigated the structure-luminescence properties of  $\text{Er}^{3+}$ -doped glasses as a function of the  $\text{BaO}/\text{MF}$  ratio, where  $\text{MF} = \text{AlF}_3$ ,  $\text{BaF}_2$ ,  $\text{MgF}_2$ , whose cation sizes are: 1.44 Å ( $\text{Ba}^{2+}$ ); 0.66 Å ( $\text{Mg}^{2+}$ ) and 0.47 Å ( $\text{Al}^{3+/IV}$ ); and 0.56 Å ( $\text{Al}^{3+/V}$ ), and 0.61 Å ( $\text{Al}^{3+/VI}$ ).

## 2. Materials and Methods

Gallo-germanate glasses doped with  $\text{Er}_2\text{O}_3$  and modified by  $\text{BaF}_2$ ,  $\text{MgF}_2$ , and  $\text{AlF}_3$  were synthesized using the conventional melt-quenching. The chemical composition of the glasses is as follows:  $(29.5-x)\text{ BaO}-60\text{ Ge}_2\text{O}_3-10\text{ Ga}_2\text{O}_3-x\text{ BaF}_2/\text{MgF}_2/\text{AlF}_3-0.5\text{ Er}_2\text{O}_3$ , where  $x = 0$  or 10 (in mol%). The glasses were labeled according to their chemical compositions. The first letters of the  $\text{BaO}$ ,  $\text{Ga}_2\text{O}_3$ , and  $\text{GeO}_2$  oxides, the molar content of erbium, and the corresponding fluoride were used to name the samples. In this paper, the following names of the samples were used: BGG0.5Er glass (gallo-germanate glass doped with 0.5 mol% of  $\text{Er}_2\text{O}_3$ ), BGG0.5Er\_BaF<sub>2</sub> glass (gallo-germanate glass doped with 0.5 mol% of  $\text{Er}_2\text{O}_3$  and modified by  $\text{BaF}_2$ ), BGG0.5Er\_MgF<sub>2</sub> glass (gallo-germanate glass doped with 0.5 mol% of  $\text{Er}_2\text{O}_3$  and modified by  $\text{MgF}_2$ ), and BGG0.5Er\_AlF<sub>3</sub> glass (gallo-germanate glass doped with  $\text{Er}_2\text{O}_3$  and modified by 0.5 mol% of  $\text{AlF}_3$ ). Each set of 6 g was prepared employing materials from SigmaAldrich (Saint Louis, MI, USA) with a purity of >99.99% ( $\text{BaO}$ ,  $\text{Ge}_2\text{O}_3$ ,  $\text{Ga}_2\text{O}_3$ ,  $\text{BaF}_2$ ,  $\text{MgF}_2$ ,  $\text{AlF}_3$ ,  $\text{Er}_2\text{O}_3$ ). The components were homogenized in

an agate mortar and then melted in a platinum crucible at 1250 °C for 1.5 h in an electric furnace. Finally, the melt was poured into a brass mold preheated at  $T_g - 30$  °C and annealed for 24 h (at  $T_g - 30$  °C) to remove residual internal stress.

The X-ray diffraction patterns were obtained using an X'Pert Pro X-ray diffractometer supplied by PANalytical (Almelo, The Netherlands) with Cu  $K\alpha_1$  radiation ( $\lambda = 1.54056$  Å) in the  $2\theta$  range of 10–90°. The X-ray tube was operated at 40 kV and 40 mA and equipped with a scintillation detector (Almelo, The Netherlands) to measure the intensity of the scattered X-rays.

The differential scanning calorimetry (DSC) curves were obtained in the range of 200–1050 °C at 10 °C/min using the SETARAM Labsys thermal analyzer (Setaram Instrumentation, Caluire, France). Measurements were carried out with an uncertainty of  $\pm 1$  °C. The glass transition  $T_g$  (onset) and the crystallization  $T_x$  temperatures were estimated at the onset and maximum of peaks, respectively. Based on these temperatures, the stability factor  $\Delta T$  was calculated.

The infrared (IR) spectra of the glasses were measured with the Fourier spectrometer (Bruker Optics-Vertex70V, Rheinstetten, Germany) using the KBr pellet technique. All spectra were recorded at 128 scans with a resolution of  $4\text{ cm}^{-1}$ . The Raman spectra of the glasses were obtained using a LabRAM HR spectrometer (HORIBA Jobin Yvon, Palaiseau, France) with an excitation wavelength of 532 nm. The diffraction grating was 1800 lines/mm. The Raman spectra were recorded with the standard spot of about  $1\text{ }\mu\text{m}$ . The IR and Raman's spectra were normalized and deconvoluted using Fityk software (0.9.8, open-source (GPL2+)).

The luminescence spectra were measured using the JobinYvon Fluoromax4 spectrophotometer (Horiba Jobin Yvon, Longjumeau, France).

### 3. Results

#### 3.1. X-ray Diffraction

The X-ray diffraction patterns of the erbium-doped glasses are shown in Figure 1. Each pattern confirmed the absence of the crystalline phase because only broad humps around 28° are observed, which corroborates the amorphous character of all the samples [26]. Moreover, pictures of the fabricated glasses are presented in the inset of Figure 1.

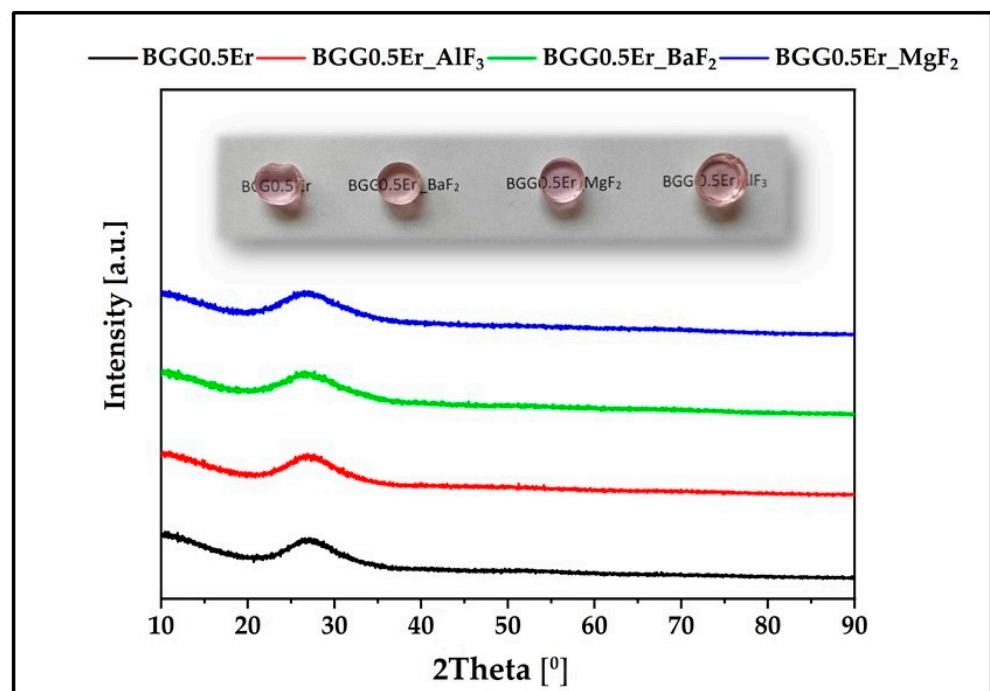
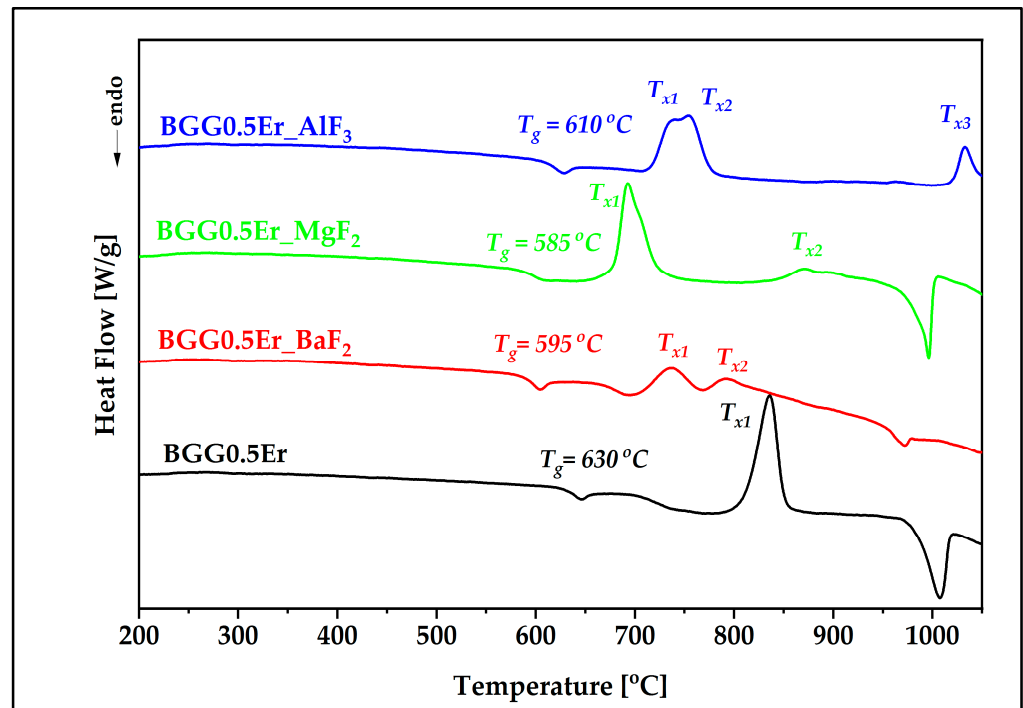


Figure 1. X-ray diffraction patterns of glasses. Pictures of the fabricated glasses (inset).

### 3.2. DSC

Differential scanning calorimetry (DSC) curves in the range of 200–1050 °C are presented in Figure 2. The DSC curves show that the exothermic behavior changes as a function of the fluoride component employed. In the case of the BGG0.5Er oxide glass, just one exothermic peak ( $T_x$ ) was observed at 836 °C while the BGG0.5Er\_BaF<sub>2</sub> (at 735 °C, 792 °C) and BGG0.5Er\_MgF<sub>2</sub> (at 642 °C, 871 °C) glasses exhibited two; and BGG0.5Er\_AlF<sub>3</sub> displayed three  $T_x$  (at 735 °C, 754 °C, and 1030 °C). These could be caused by the valence of the cations Ba<sup>2+</sup>, Mg<sup>2+</sup>, and Al<sup>3+</sup> within the matrices.



**Figure 2.** DSC curves of BGG0.5Er glass modified by BaF<sub>2</sub>, MgF<sub>2</sub>, and AlF<sub>3</sub>.

The thermal stability ( $\Delta T$ ) of a glass can be determined as the difference between  $T_{x1}$  and  $T_g$ ; the higher the  $\Delta T$  parameter, the greater the probability of successful use of the material to produce optical fibers [27,28]. As expected, the BGG0.5Er glass has the highest thermal stability ( $\Delta T = 206$  °C), which decreases with the presence of monovalent fluorine anions up to 57 °C (BGG0.5Er\_MgF<sub>2</sub> glass) [29]. The  $T_g$  and  $T_x$  temperatures of all the fluorine anions related to the first endothermic and exothermic peaks, as well as thermal stability  $\Delta T$  of the glasses, are presented in Table 1.

**Table 1.** Thermal properties of erbium-doped BGG glass modified by fluorides.

Glass	$T_g$ [°C]	$T_{x1}$ [°C]	$T_{x2}$ [°C]	$T_{x3}$ [°C]	$\Delta T$ [°C]
BGG0.5Er	630	836	-	-	206
BGG0.5Er_BaF <sub>2</sub>	595	735	792	-	140
BGG0.5Er_MgF <sub>2</sub>	585	642	871	-	57
BGG0.5Er_AlF <sub>3</sub>	610	735	754	1030	125

### 3.3. Structural Analysis

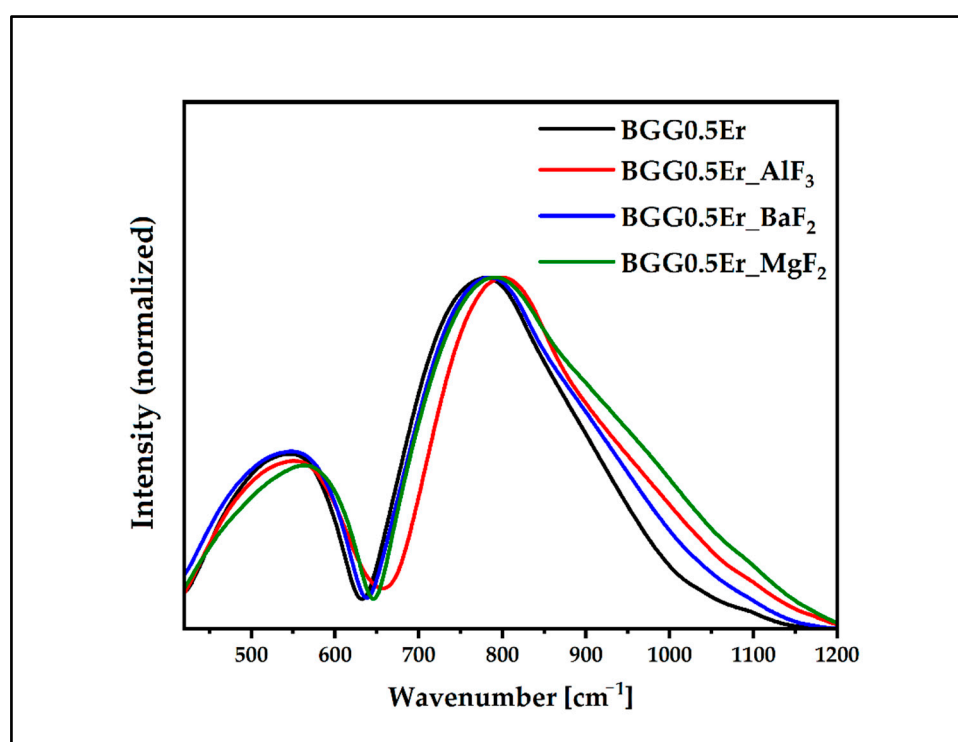
Previous reports showed that the network of the BGG glass forms a ring structure that is composed of connected GeO<sub>4</sub> and GaO<sub>4</sub> tetrahedra and surrounded by alkaline earth (Ba<sup>2+</sup>) or rare earth ions that act as charge compensators for the negative charge of the gallate tetrahedra. Depending on the M/Ga cation ratio (where M is alkali metal or



alkaline earth metals), gallium cations tend to balance the charges, forming four- or six-fold coordination units. Moreover, the Raman spectra of the gallo-germanate glasses show that four different structures describe the network of this glass ( $Q^n$ , where  $n = 0, 1, 2$ , and  $3$ , which corresponds to the number of bridging oxygen) [2,5,13,30–32]. This study discusses the glass network related to the IR and Raman spectra of glasses based on the network model mentioned above.

### 3.3.1. IR Spectra

The normalized IR spectra in the  $420\text{ cm}^{-1}$ – $1200\text{ cm}^{-1}$  range of the BGG0.5Er glass with and without the  $\text{BaF}_2$ ,  $\text{AlF}_3$ , and  $\text{MgF}_2$  compounds are shown in Figure 3. All of them exhibited two domains (bands) at the (1)  $420\text{ cm}^{-1}$ – $600\text{ cm}^{-1}$  and (2)  $650\text{ cm}^{-1}$ – $950\text{ cm}^{-1}$  regions. These do not overlap, which means that the structural modification occurred after adding the  $\text{BaF}_2$ ,  $\text{MgF}_2$ , and  $\text{AlF}_3$  compounds to the BGG0.5Er glass matrix.



**Figure 3.** Normalized IR spectra of glasses in the  $420\text{ cm}^{-1}$ – $1200\text{ cm}^{-1}$  range.

The IR spectra of the glasses were deconvoluted to investigate the changes in the BGG0.5Er glass network due to the addition of the fluoride compounds, as shown in Figures 4–7. The assignments of the components bands to the vibrations are presented in Table 2. The six-component bands were present in each spectrum. At a lower wavenumber, the two-component bands (A and B in  $490\text{ cm}^{-1}$ – $600\text{ cm}^{-1}$  range) can be attributed to bending vibrations involving X–O–X bridges (X used for Ge/Ga in tetrahedral coordination). The high-frequency region of  $650\text{ cm}^{-1}$ – $950\text{ cm}^{-1}$  is composed of four bands: C, D, E, and F (Figures 4–7). The band C at  $700\text{ cm}^{-1}$ – $730\text{ cm}^{-1}$  can be attributed to the symmetrical stretching vibration of the  $^{[6]}\text{Ge-O-}^{[6]}\text{Ge}$  bonds from the  $\text{GeO}_6$  units. The band D (at  $760\text{ cm}^{-1}$ – $800\text{ cm}^{-1}$ ) can be assigned to the asymmetrical stretching vibration of the  $^{[4]}\text{Ge-O-}^{[4]}\text{Ge}$  bonds connecting the  $\text{GeO}_4$  units. The band E (at  $850\text{ cm}^{-1}$ – $880\text{ cm}^{-1}$ ) can be attributed to the asymmetrical stretching vibration of the bridging oxygens (BO) from the  $\text{GeO}_4$  tetrahedra ( $^{[4]}\text{Ge-O-}^{[4]}\text{Ge}$ ). The last band, F, at  $950\text{ cm}^{-1}$ – $1000\text{ cm}^{-1}$  can be related to the stretching vibration of the non-bridging oxygens (NBO) of the  $\text{GeO}_4$  tetrahedra [32–36].

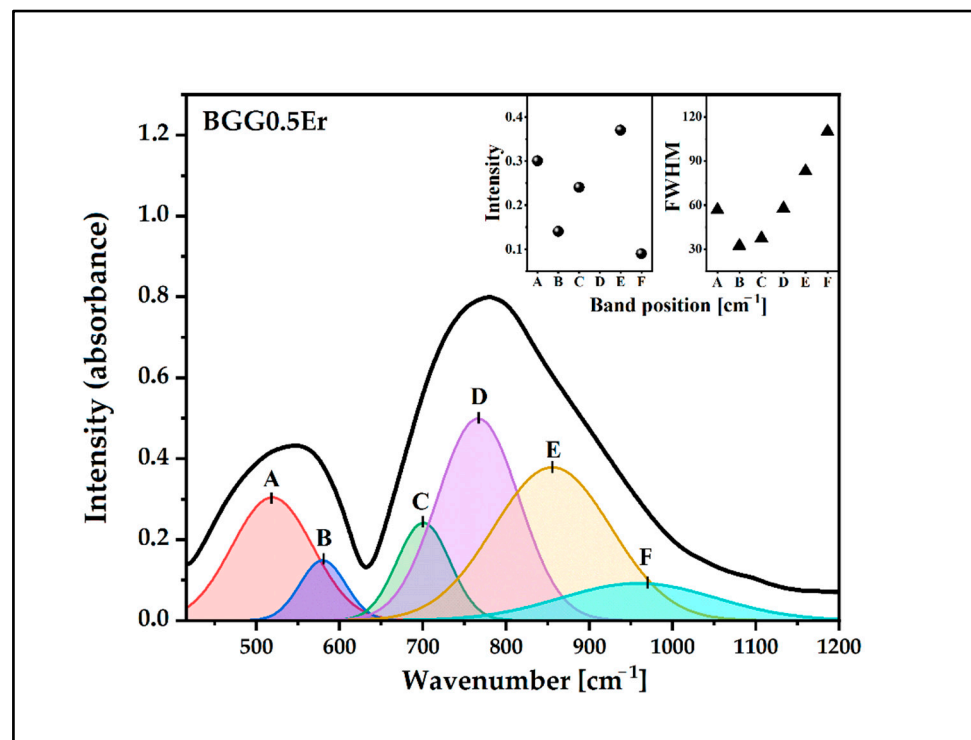


Figure 4. Deconvoluted IR spectrum of BGG0.5Er glass.

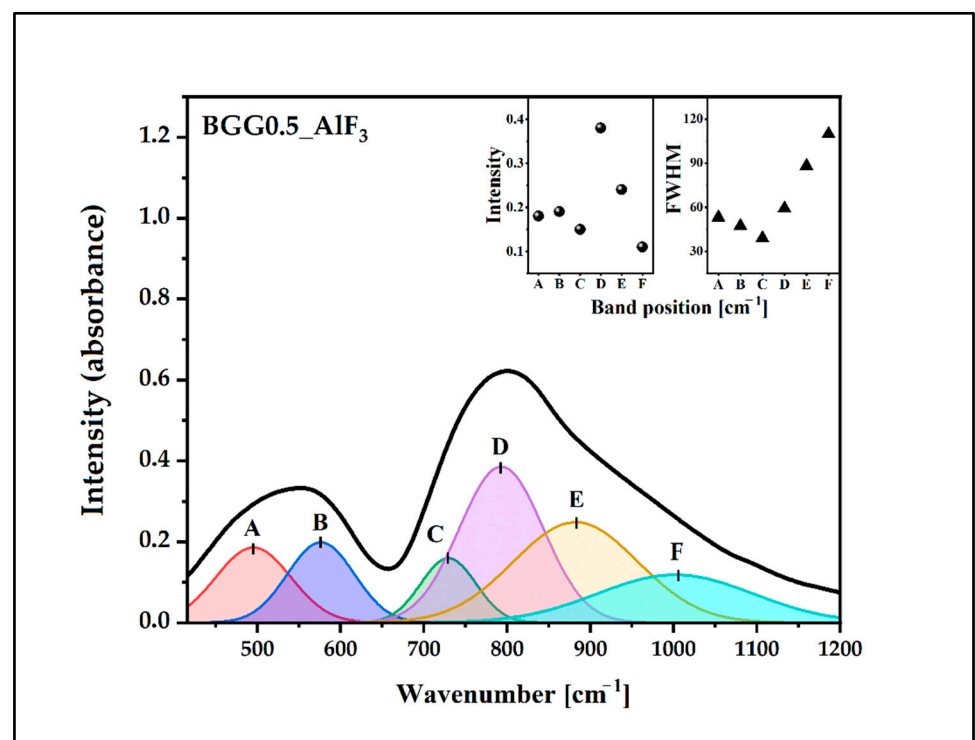


Figure 5. Deconvoluted IR spectrum of BGG0.5Er<sub>2</sub>O<sub>3</sub>-AlF<sub>3</sub> glass.

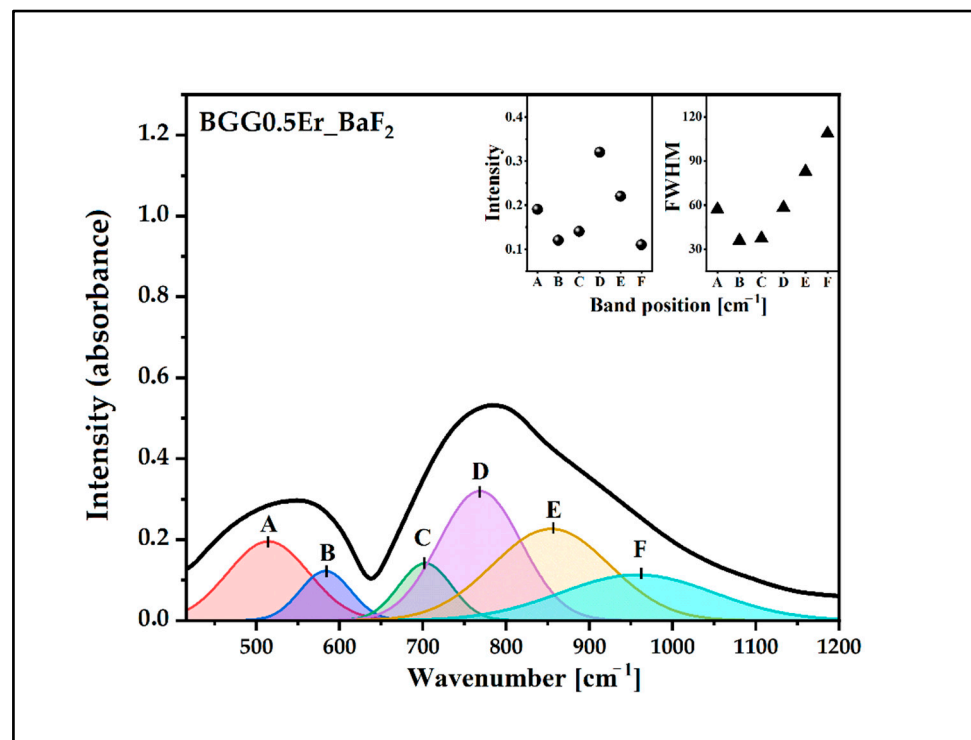


Figure 6. Deconvoluted IR spectrum of BGG0.5Er\_BaF<sub>2</sub> glass.

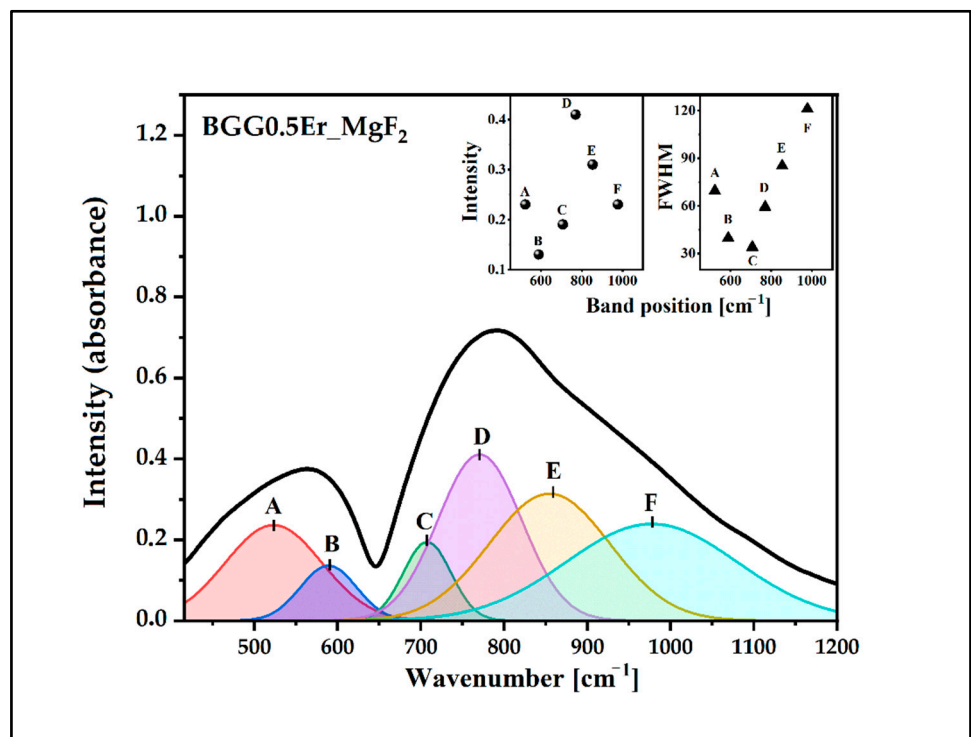
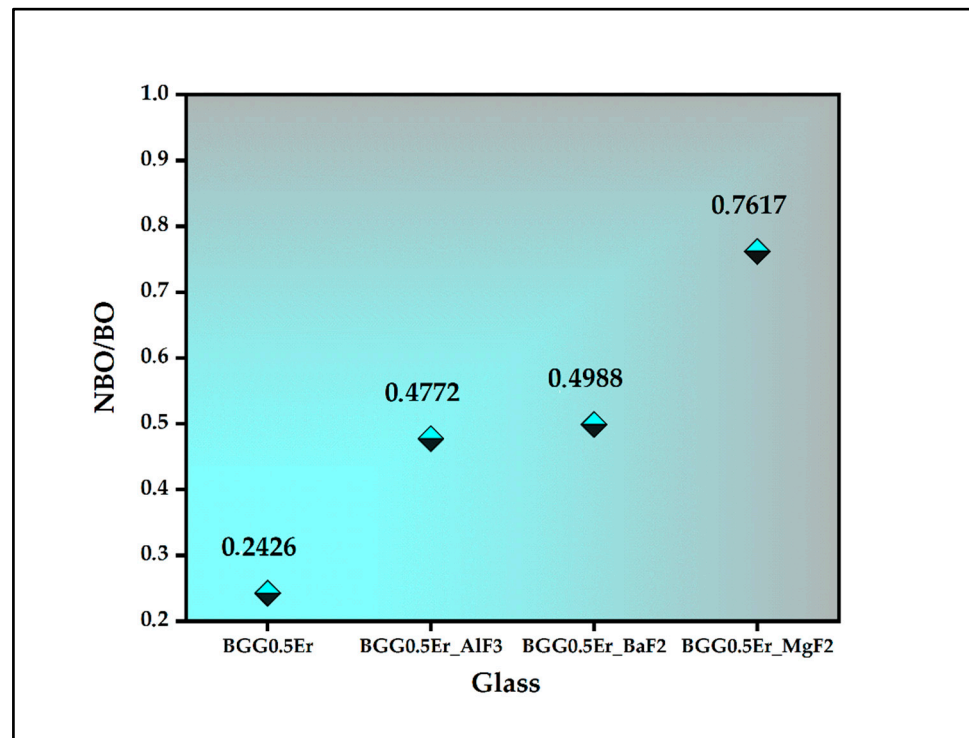


Figure 7. Deconvoluted IR spectrum of BGG0.5Er\_MgF<sub>2</sub> glass.

**Table 2.** Assignment of the IR bands.

Bands	Assignment
A	bending vibrations of X–O–X bridges (X used for Ge/Ga in tetrahedral coordination)
B	
C	symmetrical stretching vibration of the $^{[6]}\text{Ge-O-}^{[6]}\text{Ge}$ bonds from $\text{GeO}_6$ units
D	asymmetrical stretching vibration of the $^{[4]}\text{Ge-O-}^{[4]}\text{Ge}$ bonds connecting $\text{GeO}_4$ units
E	asymmetrical stretching vibration of the bridging oxygens (BO) from $\text{GeO}_4$ tetrahedra
F	stretching vibration of the non-bridging oxygens (NBO) of $\text{GeO}_4$ tetrahedra

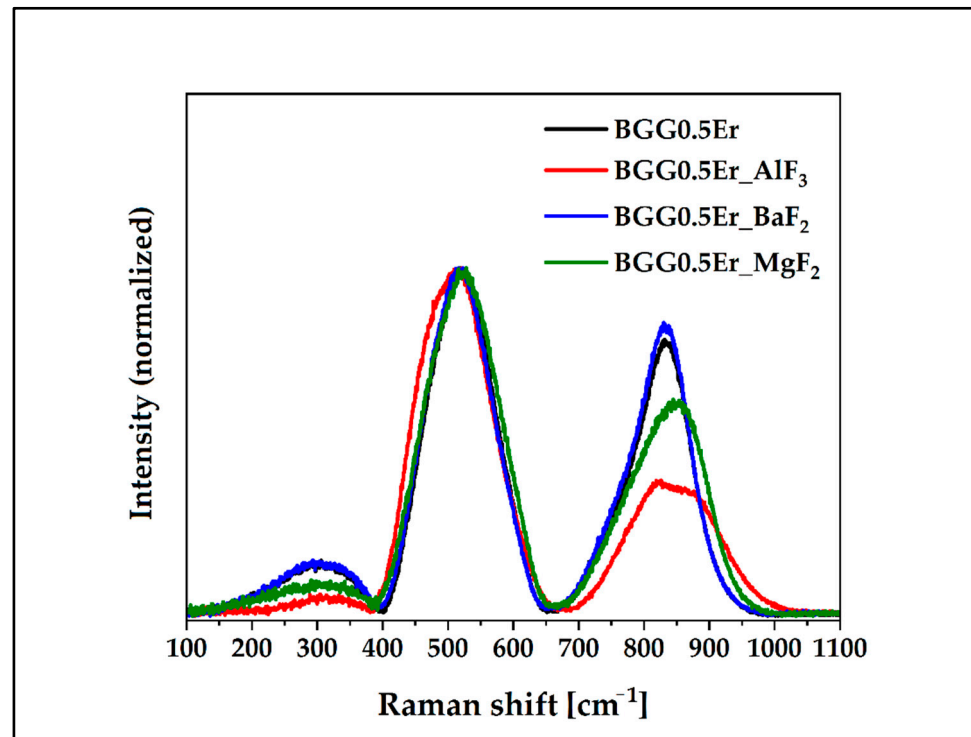
The parameters of the component bands are presented in the inset of Figures 4–7 (the intensity and full width at half maximum (FWHM)). The assessment of the bands in the IR spectra indicates that the intensity of the bands from the BO and NBO vibrations change when the fluorides are added to the matrix. These promote the formation of NBO to the detriment of the bridging oxygens (BO) in the  $\text{GeO}_4$  tetrahedrons. As a result, the degree of polymerization of the BGG0.5Er glass network decreased while its NBO/BO ratio was 0.24. However, the NBO/BO ratio of the samples with cation size increases is as follows:  $\langle \text{MgF}_2 (0.76) \rangle \text{BaF}_2 (0.49) \rangle \text{AlF}_3 (0.47)$  (Figure 8), which is in concordance with the results obtained by Guérineau et al., in which the addition of the  $\text{Y}_2\text{O}_3$  and  $\text{La}_2\text{O}_3$  in a BGG system caused the appearance of more NBO in the germanium and gallate polyhedra [5].

**Figure 8.** The ratio of the NBO/BO.

### 3.3.2. Raman Spectra

The structural compositions of all composites were completed using Raman spectroscopy. Figure 9 presents the normalized Raman spectra for glasses in the  $100\text{--}1100\text{ cm}^{-1}$ . The three Raman signatures in the maximum at  $300\text{ cm}^{-1}$ ,  $500\text{ cm}^{-1}$ , and  $850\text{ cm}^{-1}$  are presented in Figure 9. Moreover, the two bands in the  $200\text{ cm}^{-1}\text{--}400\text{ cm}^{-1}$  and  $650\text{ cm}^{-1}\text{--}1100\text{ cm}^{-1}$  ranges have various intensities. Furthermore, the FWHM of the

bands have different values, indicating that the modification of the structure occurred when the fluoride compounds were added.



**Figure 9.** Normalized Raman spectra of glasses in the  $100\text{ cm}^{-1}$ – $1100\text{ cm}^{-1}$  range.

The deconvoluted Raman spectra of the glasses were presented in Figures 10–13. The assignment of the vibrations observed in the components bands (seven) is presented in Table 3. The component bands (G–M) are presented in each decomposed Raman spectrum. Additionally, the band X appeared in the decomposed Raman spectrum of the BGG0.5Er\_AlF<sub>3</sub> glass. The band G (at around  $250\text{ cm}^{-1}$ – $300\text{ cm}^{-1}$ ) can be assigned to the bending vibration of the Ge–O–Ge bonds of the Ge(2) units. The band H at  $320\text{ cm}^{-1}$ – $350\text{ cm}^{-1}$  can be attributed to the Ge,Ga–O–Ba vibration. The band I (at  $450\text{ cm}^{-1}$ – $460\text{ cm}^{-1}$ ) is related to the symmetrical stretching vibration of the Ge,Ga–O–Ge,Ga bonds with a four-membered GeO<sub>4</sub>/GaO<sub>4</sub> ring. The band J (at  $500\text{ cm}^{-1}$  to  $520\text{ cm}^{-1}$ ) is assigned to the vibration of BO (GeO<sub>4</sub>/GaO<sub>4</sub>) in three-membered rings. The band K (at around  $560\text{ cm}^{-1}$ – $580\text{ cm}^{-1}$ ) can be attributed to the symmetrical stretching vibration of the GeO<sub>6</sub> octahedral. The next band, L, (at  $740\text{ cm}^{-1}$  to  $770\text{ cm}^{-1}$ ) is related to the symmetrical stretching vibration of the NBO (Ge–O-) of Ge(2) units. The band X at around  $812\text{ cm}^{-1}$  in the spectrum of the BGG0.5Er\_AlF<sub>3</sub> glass can be assigned to the symmetric stretching vibration of the Al–O–Al in the Al(4) units. The last band in each decomposed spectrum of glasses (M, at  $830\text{ cm}^{-1}$ – $860\text{ cm}^{-1}$ ) corresponds to the symmetric stretching vibration of the NBO (Ge–O-) of the Ge(3) units [34,37–42]. Based on the Raman spectra studies, we assume that the addition of the fluoride compounds to the BGG\_0.5Er glass results in decreases in the Ge(3) units at the expense of an increase in the Ge(2) units.



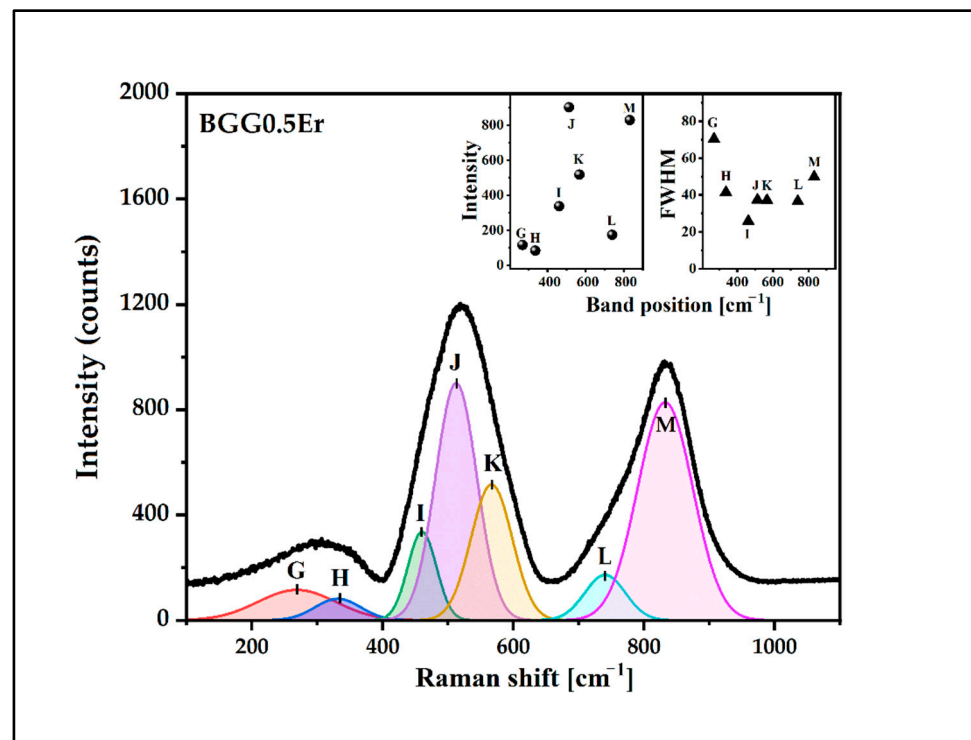


Figure 10. Deconvoluted Raman spectrum of BGG0.5Er glass.

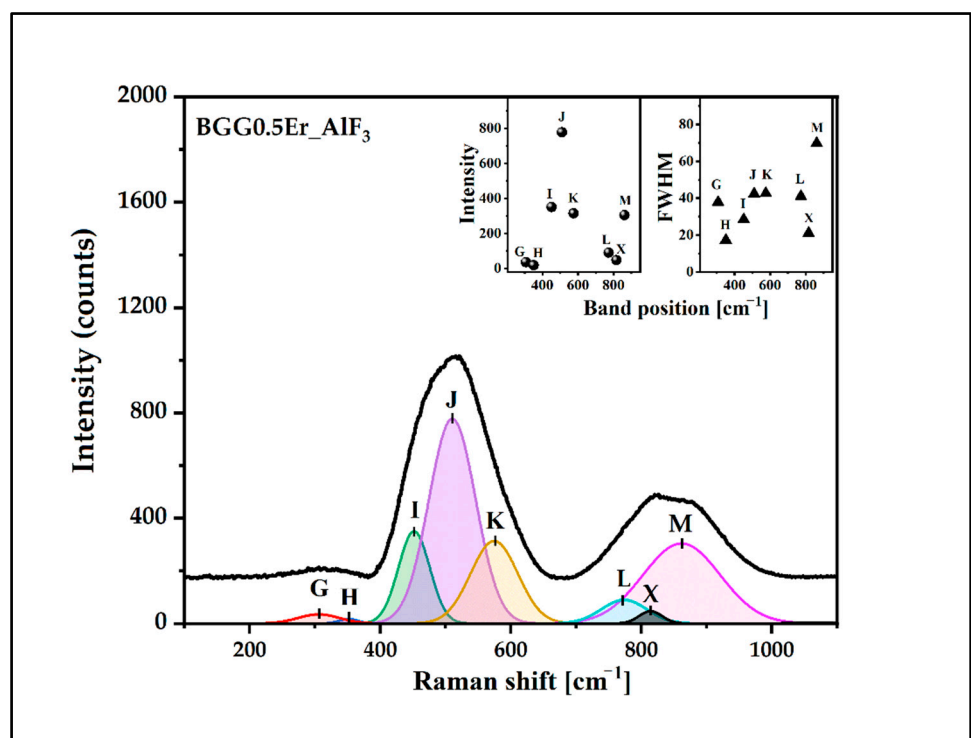


Figure 11. Deconvoluted Raman spectrum of BGG0.5Er\_AIF<sub>3</sub> glass.

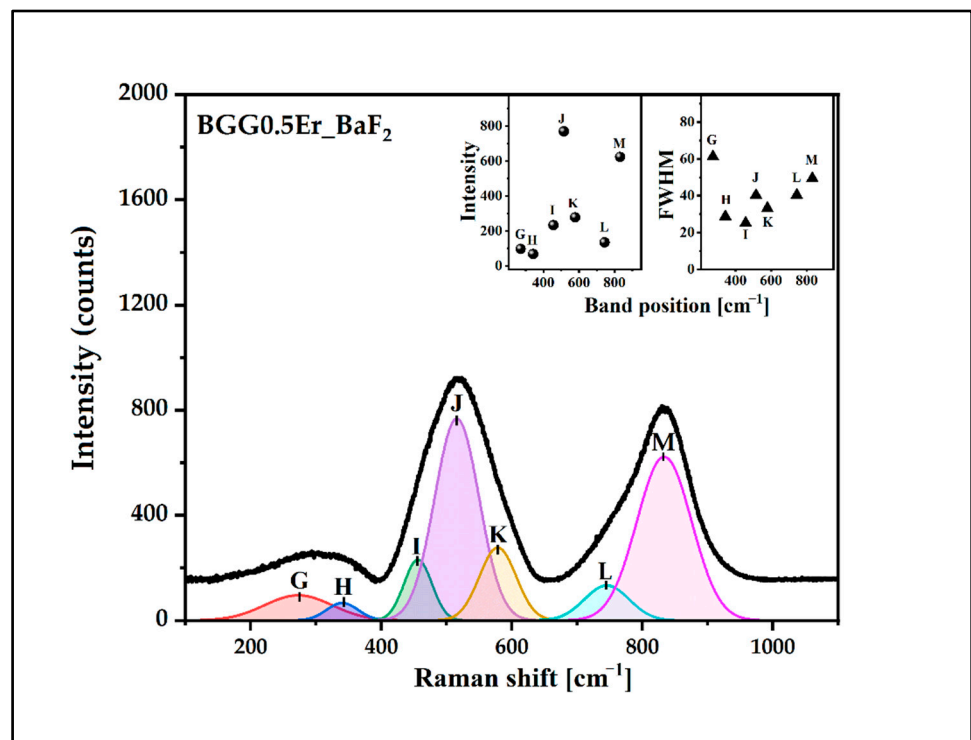


Figure 12. Deconvoluted Raman spectrum of BGG0.5Er\_BaF<sub>2</sub> glass.

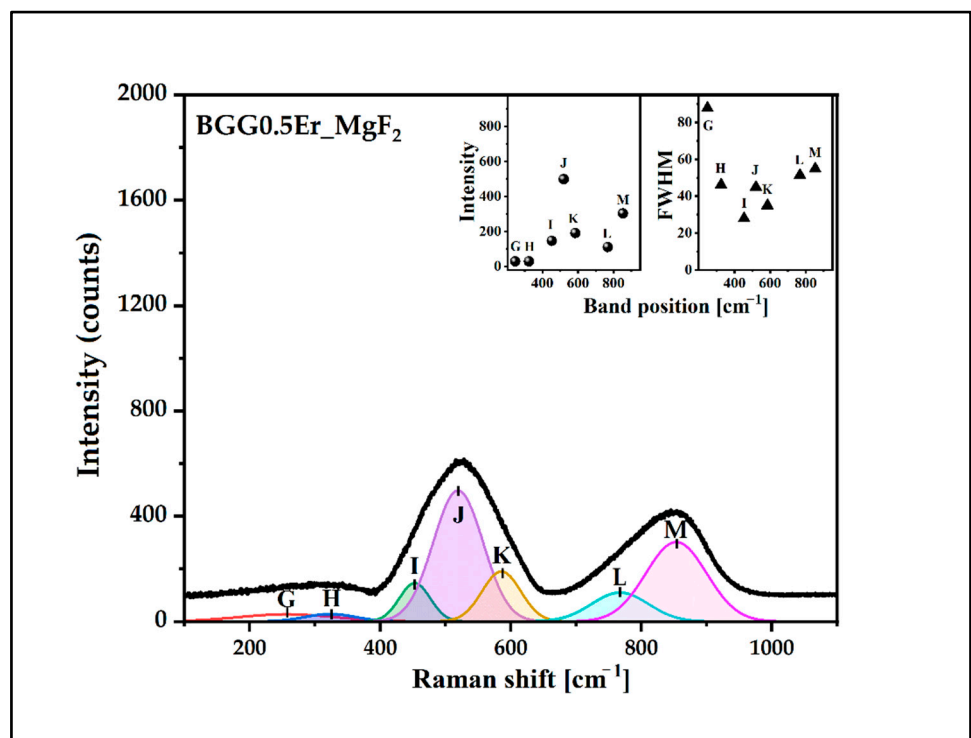


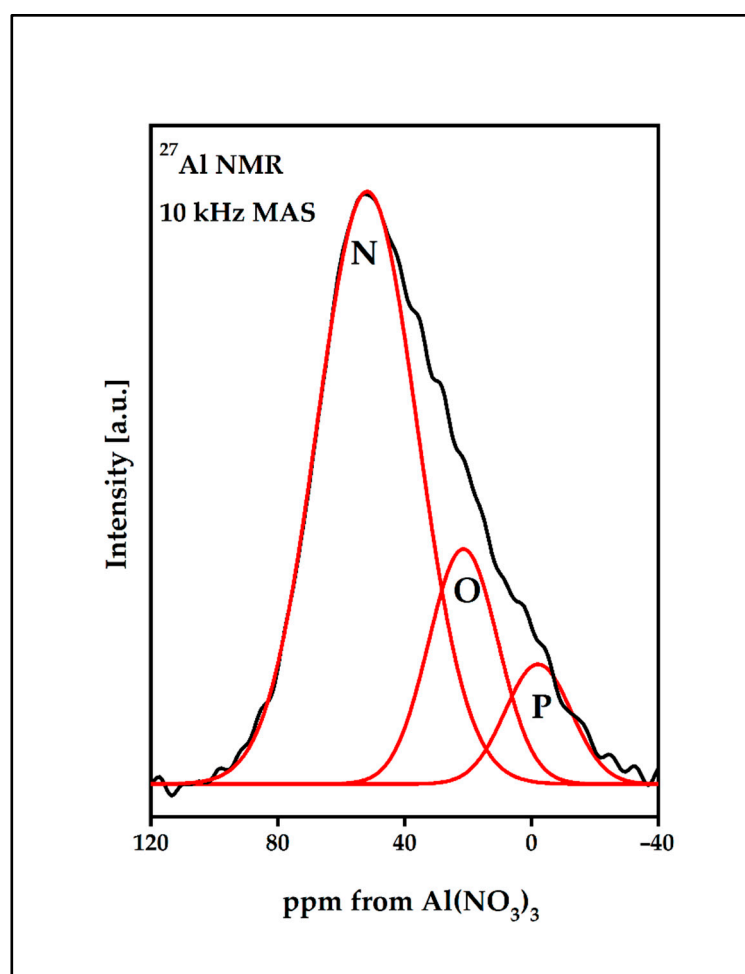
Figure 13. Deconvoluted Raman spectrum of BGG0.5Er\_MgF<sub>2</sub> glass.

**Table 3.** Assignment of the bands in Raman spectra of glasses.

Bands	Assignment
G	bending vibration of the Ge-O-Ge bonds of Ge(2) units
H	Ge,Ga-O-Ba vibration
I	symmetrical stretching vibration of the Ge,Ga-O-Ge,Ga bonds with a 4-membered GeO <sub>4</sub> /GaO <sub>4</sub> ring
J	the vibration of BO (GeO <sub>4</sub> /GaO <sub>4</sub> ) in 3-membered rings
K	symmetrical stretching vibration of the GeO <sub>6</sub> octahedral
L	symmetrical stretching vibration of the NBO (Ge-O-) of Ge(2) units
M	symmetrical stretching vibration of the NBO (Ge-O-) of Ge(3) units
X	symmetric stretching vibration of the Al-O-Al in Al(4) units

### 3.3.3. <sup>27</sup>Al MAS NMR Spectrum Analysis

Figure 14 presents the <sup>27</sup>Al MAS-NMR spectrum of the BGG0.5Er<sub>2</sub>AlF<sub>3</sub> glass. The analyzed spectrum shows a primary resonance with a maximum in the −3 ppm (band N), 20 ppm (band O), and 50 ppm (band P), which is characteristic of a six-, five-, and four-coordinated aluminum, respectively [43]. The parameters of the components band are given in Table 4.

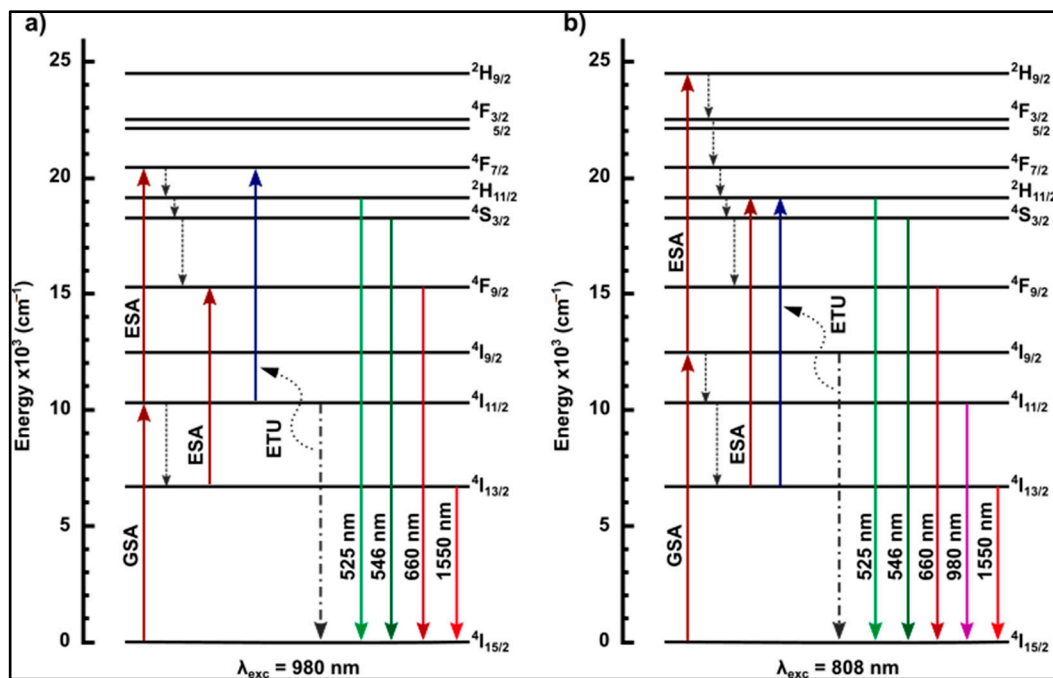
**Figure 14.** <sup>27</sup>Al MAS-NMR spectrum of BGG0.5Er<sub>2</sub>AlF<sub>3</sub> glass.

**Table 4.** Deconvolution of  $^{27}\text{Al}$  MAS-NMR spectrum.

Glass	Peak Position [ppm]	FWHM [ppm]	Relative Intensity [%]
BGG0.5Er <sub>2</sub> AlF <sub>3</sub>	52.6	37.1	71
	22.2	25.7	20
	−1.3	24.5	9

### 3.4. Luminescence Properties

The luminescence measurements were performed by pumping the glasses with the two characteristic erbium absorption bands (980 nm and 808 nm) using a high-power semiconductor laser diode. The first one corresponds to the  $^4\text{I}_{15/2} \rightarrow ^4\text{I}_{11/2}$  energy transition (the ground state absorption phenomenon) and is widely used for the excitation of rare earth ions doped with glasses or optical fibers due to the high absorption cross-section (Figure 15a). The second absorption band is characterized by a lower absorption cross-section parameter, which corresponds to the  $^4\text{I}_{15/2} \rightarrow ^4\text{I}_{9/2}$  transition from GSA (Figure 15b). In this work, we analyze the energy flow in the context of two transition channels—Ch<sub>980</sub> ( $^4\text{I}_{15/2} \rightarrow ^4\text{I}_{11/2}$ ) and Ch<sub>808</sub> ( $^4\text{I}_{15/2} \rightarrow ^4\text{I}_{9/2}$ ). After GSA, the erbium ions in the Ch<sub>808</sub> could non-radiatively relax to the  $^4\text{I}_{11/2}$ 's lower energy level, and therefore, another non-radiative relaxation to the  $^4\text{I}_{13/2}$  state can occur in both channels. Finally, the radiative transition  $^4\text{I}_{13/2} \rightarrow ^4\text{I}_{15/2}$  occurs, resulting in a strong luminescence band at 1.55  $\mu\text{m}$ . Simultaneously, the erbium ions could absorb additional energy after the GSA process, thereby inducing a transition to higher energy states. Excited state absorption (ESA) and energy Transfer up-conversion (ETU) occur in both channels and result in  $^4\text{I}_{11/2} \rightarrow ^4\text{F}_{7/2}$ , (Ch<sub>980</sub>),  $^4\text{I}_{9/2} \rightarrow ^2\text{H}_{9/2}$  (Ch<sub>808</sub>), and  $^4\text{I}_{13/2} \rightarrow ^2\text{H}_{11/2}$  (Ch<sub>808</sub>) transitions [44]. Afterward, the non-radiative relaxation processes can cause erbium ions to move to lower energy levels where it becomes possible to observe the radiative transitions in both channels:  $^2\text{H}_{11/2} \rightarrow ^4\text{I}_{15/2}$  (525 nm),  $^4\text{S}_{3/2} \rightarrow ^4\text{I}_{15/2}$  (546 nm), and  $^4\text{F}_{9/2} \rightarrow ^4\text{I}_{15/2}$  (660 nm). The luminescence spectra observed in the near-infrared and visible range are the result of the energy flow of the erbium ions in down- and up-conversion processes. Since both phenomena are mutually competitive, it was possible to observe changes in the intensity of the luminescence in particular bands during modification of the composition of the matrix [29,45]. Further analysis will allow for the determination of energy flow channels as a function of different fluoride compounds in the glass matrix.



**Figure 15.** Energy level diagrams of  $\text{Er}^{3+}$ -doped gallo-germanate glasses under laser excitation at (a) 980 nm and (b) 808 nm. GSA, ESA, non-radiative, and possible luminescence transitions have been indicated.

### 3.4.1. Luminescence Results under the 980 nm Excitation Pump

Figures 16 and 17 present the luminescence effect of using fluoride modifiers ( $\text{BaF}_2$ ,  $\text{MgF}_2$ ,  $\text{AlF}_3$ ) in the matrix. It is possible to observe that the samples with the fluoride components showed an enhancement of the emission intensity in the near-infrared range located at 1400–1700 nm (Figure 16), which is related to the radiative energy transition  $^4\text{I}_{13/2} \rightarrow ^4\text{I}_{15/2}$ . Regarding the visible range from 500 to 700 nm (Figure 17), three luminescence bands at 525 nm ( $^2\text{H}_{11/2} \rightarrow ^4\text{I}_{15/2}$ ), 546 nm ( $^4\text{S}_{3/2} \rightarrow ^4\text{I}_{15/2}$ ), and 660 nm ( $^4\text{F}_{9/2} \rightarrow ^4\text{I}_{15/2}$ ) were identified. All bands of the visible range exhibited a slight increase in the luminescence intensity, except for the glassy matrix containing  $\text{MgF}_2$ , for which the decrease was significant at 546 nm and 660 nm. To explain this phenomenon, it is necessary to analyze the possible energy transitions inside the erbium ions during pumping radiation using a 980 nm light source (Figure 15a). After the ground state absorption, excited state absorption, and energy transfer up-conversion processes, erbium ions from the  $^4\text{F}_{7/2}$  can non-radiatively transit to the  $^2\text{H}_{11/2}$  excited energy level, from where a radiative transition to the  $^4\text{I}_{15/2}$  ground level can take place, resulting in the emission of an electromagnetic wave with a wavelength at 525 nm. On the other hand, excited erbium ions can transit non-radiatively from  $^2\text{H}_{11/2}$  to the  $^4\text{S}_{3/2}$  and  $^4\text{F}_{9/2}$  lower energy levels; from here, there can be radiative transitions to the ground energy level, which are responsible for generating the two visible radiative bands at 546 nm and 660 nm, respectively [24,46].



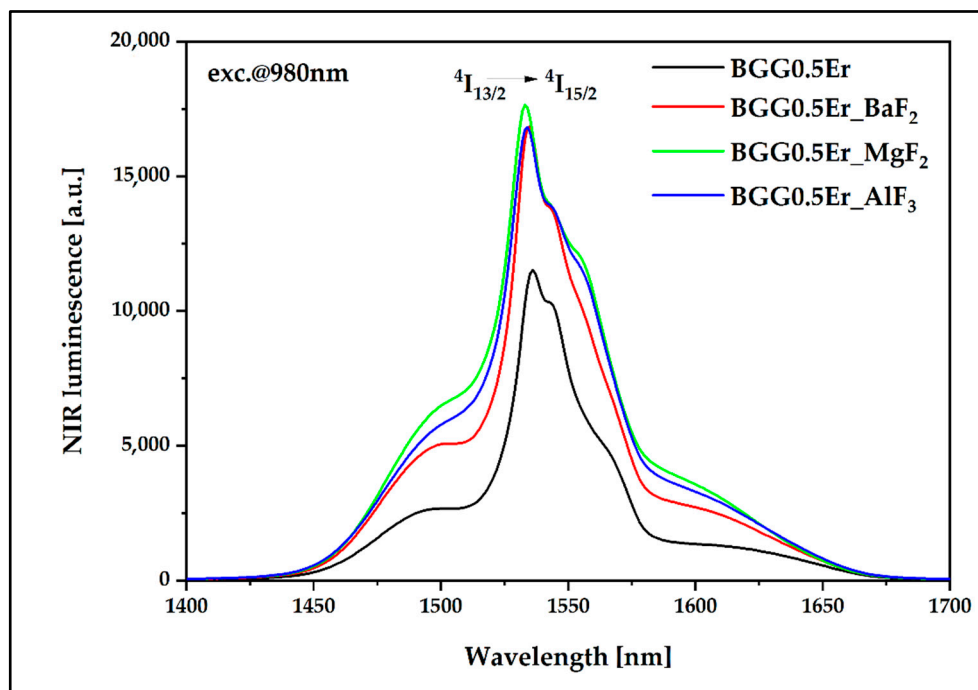


Figure 16. Luminescence spectra of Er<sup>3+</sup>-doped BGG glass modified by different fluoride compounds under 980 nm laser excitation.

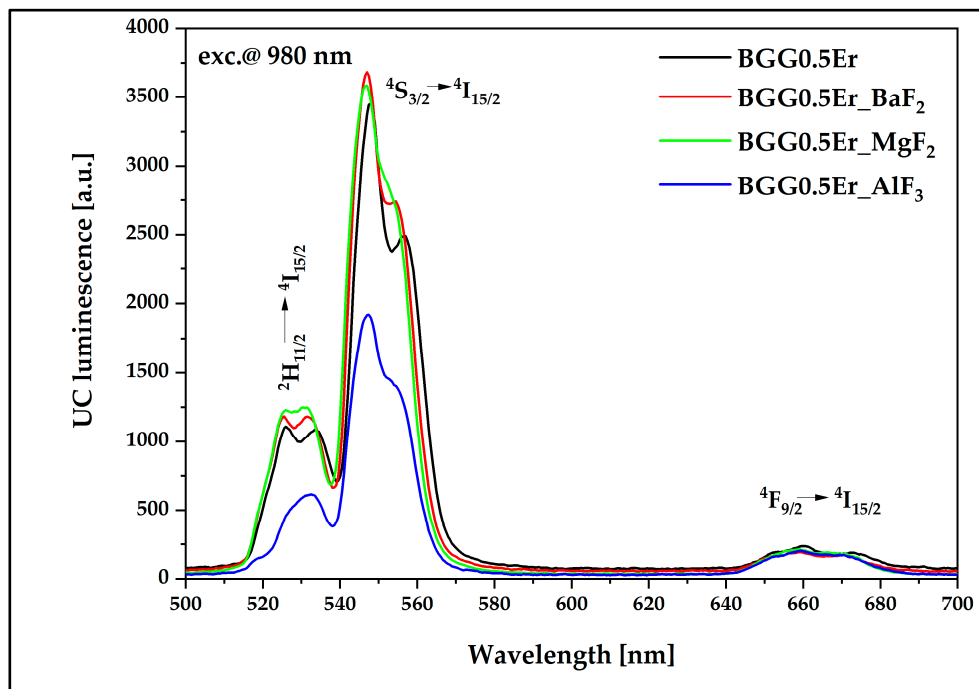


Figure 17. UC luminescence of Er<sup>3+</sup>-doped BGG glass modified by different fluoride compounds under 980 nm laser excitation.

The only variable in this work is the introduction of fluorides as glass-forming components. Barium and magnesium fluorides have practically no effect on the energy flow channels in the visible range compared to the BGG0.5Er, while the addition of aluminum fluoride reduces the energy flow channel from <sup>4</sup>F<sub>7/2</sub> to lower energy levels. One bridging oxygen anion in the glass network is replaced by two non-bridging fluorine anions when fluorine is added to the oxide glass. It is well known that an increasing number of non-

bridging oxides (NBO) in a glass structure leads to a decrease in phonon energy of the host glass and promotes the up-conversion mechanisms [47]. However, due to the smallest ionic radius ( $0.51 \text{ \AA}$ ) and the highest field strength ( $11.53 \text{ \AA}^{-2}$ ) of  $\text{Al}^{3+}$  among the other analyzed fluorides, the aluminum ions modify, similarly to glass-forming ions in the gallo-germanate glass network. The absorbance band (labeled as X) is observed in the Raman spectrum of the BGG0.5Er<sub>2</sub>AlF<sub>3</sub> glass (Figure 11). The presence of this band indicates that the chemical bonds are stronger in the glass network and the maximum phonon energy is slightly shifted towards a higher value. Aluminum-glass network atoms reduce the probability of  $^2\text{H}_{11/2} \rightarrow ^4\text{I}_{15/2}$  and  $^4\text{S}_{3/2} \rightarrow ^4\text{I}_{15/2}$  radiative transitions and promote a non-radiative energy transition [28,47].

To take a closer look at the process of energy conversion from the IR range to the visible range, we analyzed the luminescence signal in the 525 nm ( $\text{Er}^{3+}: ^2\text{H}_{11/2} \rightarrow ^4\text{I}_{15/2}$ ), 546 nm ( $\text{Er}^{3+}: ^4\text{S}_{3/2} \rightarrow ^4\text{I}_{15/2}$ ), and 660 nm ( $\text{Er}^{3+}: ^4\text{F}_{9/2} \rightarrow ^4\text{I}_{15/2}$ ) emission bands as a function of the pump radiation intensity ( $\lambda_{\text{exc}} = 980 \text{ nm}$ ). The obtained energy slope values indirectly allow for the determination of the  $E_{\text{IR}} \rightarrow E_{\text{VIS}}$  conversion efficiency. Considering the 525 nm band, the BGG0.5Er glass can be characterized by the smallest value of the slope, equal to 1.08, while the highest value of 1.45 was determined for the BGG0.5Er<sub>2</sub>MgF<sub>2</sub> glass (Figure 18). In a situation where there are no unfavorable depopulation processes (non-radiative transitions—multiphonon; energy migration; luminescence quenching), the conversion values are equal to 2.0 due to the emission occurring via two-photon absorption—GSA and ESA [14,48]. A similar correlation is observed in the 546 nm luminescence band; the slope values are in the range from 1.27 in the BGG0.5Er sample to 1.46 in the BGG0.5Er<sub>2</sub>MgF<sub>2</sub> glass (Figure 19).

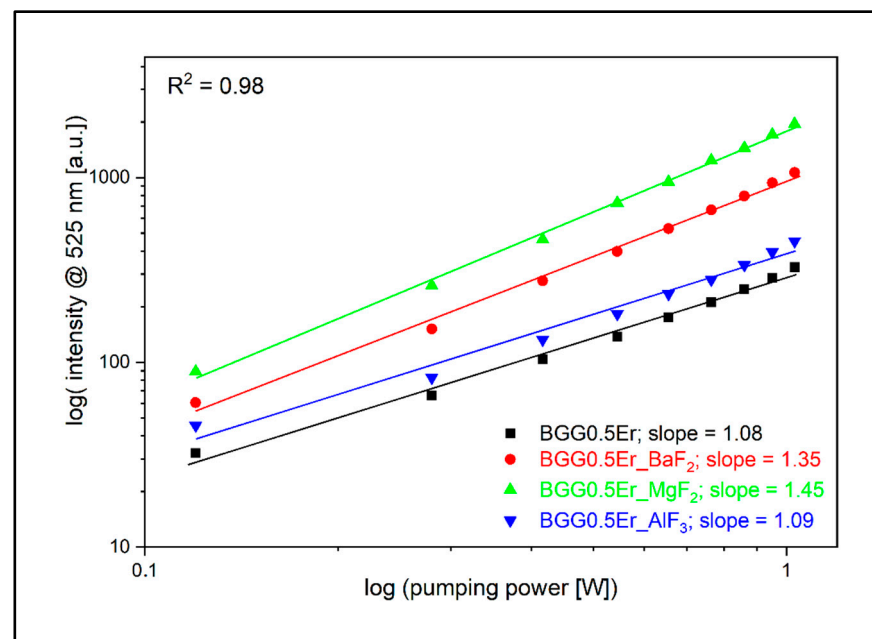
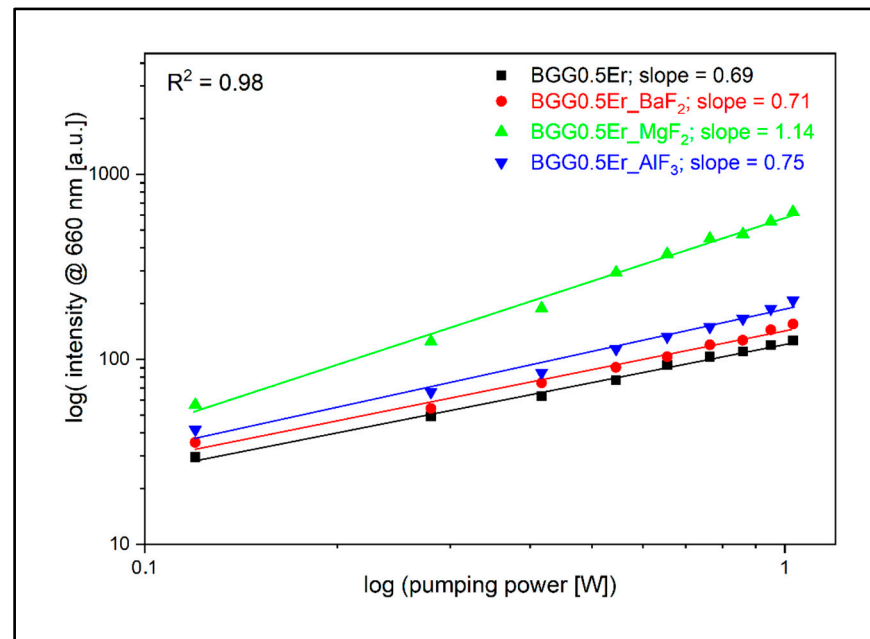


Figure 18. Log–log plot of up-conversion emission at 525 nm of fabricated glasses.



**Figure 19.** Log–log plot of up-conversion emission at 546 nm of fabricated glasses.

Significantly smaller values of the slope parameter were observed during the analysis of the pump radiation power's impact on the emission intensity at the wavelength of 660 nm. Although, as in the investigation of the other bands in the visible range, the minimum value of the slope is characterized by the sample BGG0.5Er, which equals 0.69, and the largest value of 1.14 is characterized by the sample BGG0.5Er\_MgF<sub>2</sub>. Erbium ions after GSA and a non-radiative Er<sup>3+</sup>: <sup>4</sup>I<sub>11/2</sub> → <sup>4</sup>I<sub>13/2</sub> transition relax to the <sup>4</sup>I<sub>15/2</sub> ground level and emit radiation at a wavelength of 1.55 μm. Simultaneously, the excited state absorption Er<sup>3+</sup>: <sup>4</sup>I<sub>11/2</sub> → <sup>4</sup>F<sub>9/2</sub> can occur (Figure 15a). Due to the competitive nature of these phenomena, the rate of the <sup>4</sup>F<sub>9/2</sub> (due to the ESA process) level population is limited by the effective Er<sup>3+</sup>: <sup>4</sup>I<sub>13/2</sub> → <sup>4</sup>I<sub>15/2</sub> radiative transition, as evidenced by the luminescence research and, further, by the obtained low values of the slope parameter for the 660 nm emission band (Figure 20).

The obtained slope parameters in our research prove the existence of harmful multiphonon depopulation processes. Glass modified with MgF<sub>2</sub> is characterized by the highest luminescence for both the IR and visible range among all of the examined samples. Erbium incorporated into the immediate surroundings of magnesium ions causes an increase in the ratio of the probability of the occurrence of radiative transitions in comparison to non-radiative transitions, which is also particularly evident from the obtained slope parameter values. The predominant non-radiative transitions in other matrices result in slope values at levels below 1.0. The addition of fluorides as glass-forming components and further incorporation of F<sup>−</sup> anions into the glass reduce this feature as the maximum phonon energy decreases in comparison to the BGG0.5Er, a glass based only on oxides [46,47]. The highest energy slope value has been observed in glass with the magnesium fluoride component due to the influence of Mg<sup>2+</sup> cations on the depolymerization of the BGG0.5Er glass structure.

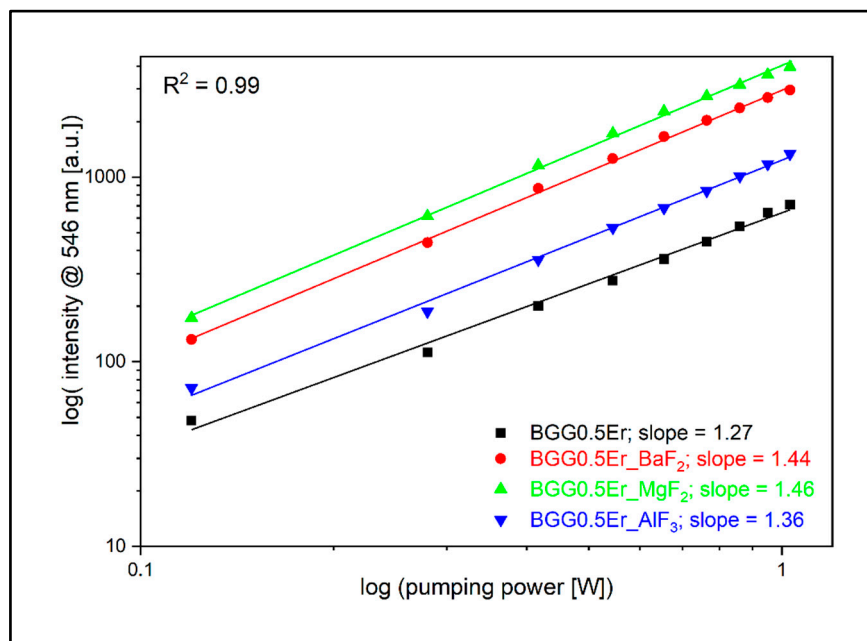


Figure 20. Log–log plot of up-conversion emission at 660 nm of fabricated glasses.

### 3.4.2. Luminescence Results under the 808 nm Excitation Pump

During further research, the synthesized glass matrices were investigated in terms of the luminescent properties under excitation radiation at 808 nm. Regarding the emission in the near-IR range (Figure 21), the profile of the luminescence spectrum is identical to that observed when pumping at 980 nm. At the same time, it is visible that, in the samples with the fluoride glass-forming components, the probability of the energy flow channel related to the occurring  $^4I_{13/2} \rightarrow ^4I_{15/2}$  radiative transition is higher than in the glass matrix based solely on oxides (BGG0.5Er).

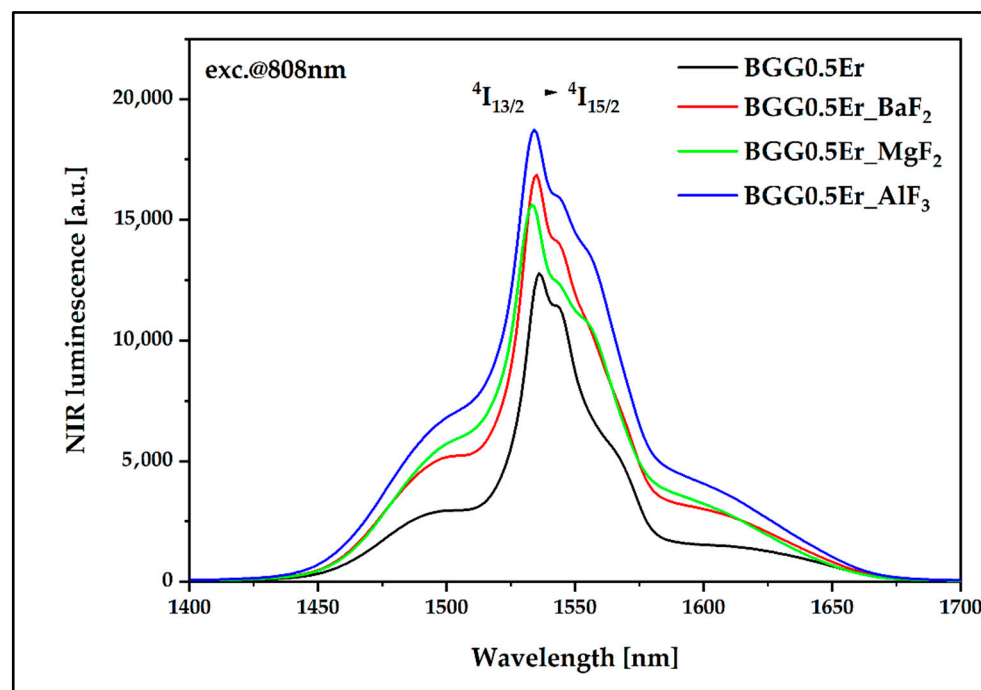
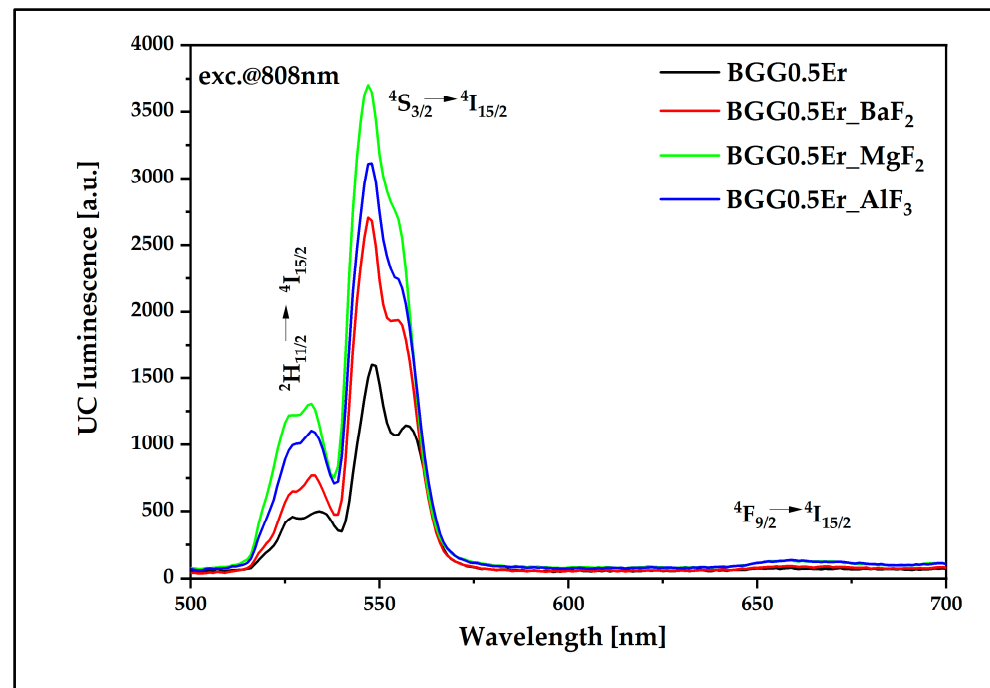


Figure 21. Luminescence spectra of Er<sup>3+</sup>-doped BGG glass modified by different fluoride compounds under 808 nm laser excitation in the 1400–1700 nm range.

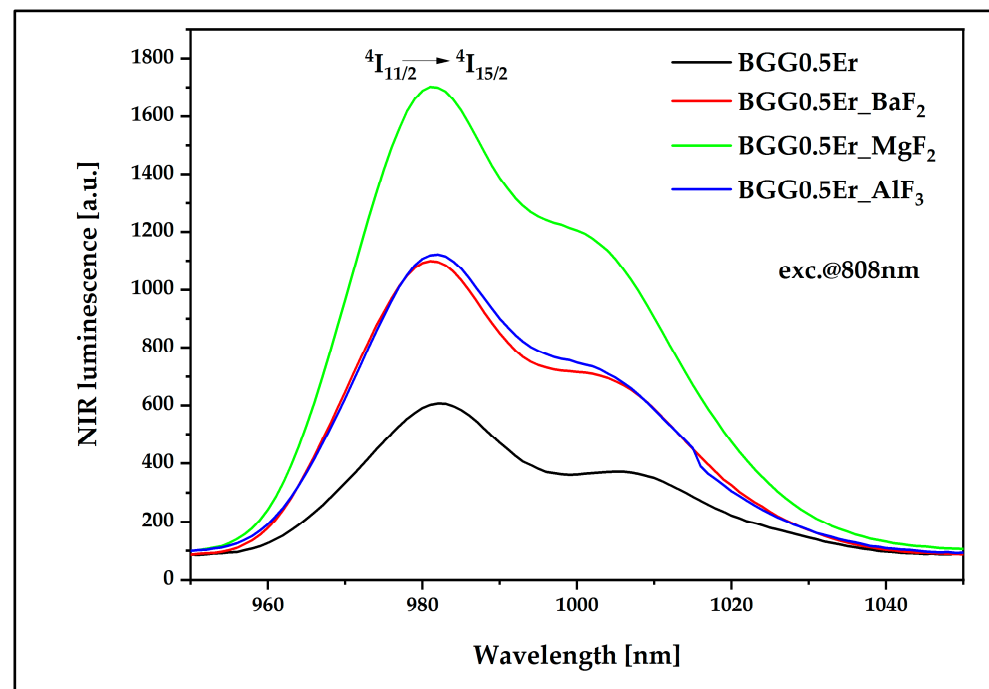
In the visible spectrum range, we observed a significant decrease in the signal at 660 nm, which is related to the radiative transition  ${}^4F_{9/2} \rightarrow {}^4I_{15/2}$  (Figure 22). After the GSA and ESA processes, the probability of emitting energy from the upper levels ( ${}^2H_{11/2}$  and  ${}^4S_{3/2}$ ) to the radiative transitions ( ${}^4I_{15/2}$ —ground level) is higher than the probability of a non-radiative transition ( ${}^4F_{9/2}$  lower energy level), as observed in Figure 15b. The presence of fluorides in the glass matrix leads to an almost complete blockage of the non-radiative relaxation channel, simultaneously promoting the channels associated with luminescent transitions [24,46]. Glass with the addition of  $MgF_2$  is characterized by the highest luminescence intensity in the emission bands centered at the wavelengths of 525 nm and 546 nm, while the base-oxygen glass BGG0.5Er has a smaller probability for luminescence transitions in the visible range.



**Figure 22.** UC luminescence of  $Er^{3+}$ -doped BGG glass modified by different fluoride compounds under 808 nm laser excitation.

To fully analyze the energy flow channels, the near-infrared luminescence research was performed in the band at 980 nm, which is related to the radiative transition  $Er^{3+}: {}^4I_{11/2} \rightarrow {}^4I_{15/2}$ . The results presented in Figure 23 indicate the opening of this emission channel, which is associated with the addition of fluorides into the glass matrix. In particular, the influence of  $MgF_2$  on the efficiency of the energy conversion  $\eta$  in this band is significantly positive since it shows the highest emission intensity among all of the synthesized samples.





**Figure 23.** Near-infrared luminescence spectra of Er<sup>3+</sup>-doped BGG glass modified by different fluoride compounds under 808 nm laser excitation.

#### 4. Discussion

AlF<sub>3</sub>, BaF<sub>2</sub>, and MgF<sub>2</sub> were substituted for BaO in the BaO-Ga<sub>2</sub>O<sub>3</sub>-GeO<sub>2</sub> glass doped with erbium ions to change the local structure of the gallo-germanate glass (BGG). According to the obtained results, by adding AlF<sub>3</sub>, BaF<sub>2</sub>, and MgF<sub>2</sub> into the glass host, the luminescence properties of erbium ions are enhanced. Based on infrared and Raman spectroscopies, it has been proven that the presence of AlF<sub>3</sub>, BaF<sub>2</sub>, and MgF<sub>2</sub> in the BGG glass host causes an increase in the number of non-bridging oxygens due to the depolymerization of the gallo-germanate glass network. It is well-known that the field strength of cations strongly influences the structure of glasses and their suitability for various applications. The changes in the BGG glass structure can be explained as relating to the effects of network-modifying cation field strength (cation field strength =  $Z/r^2$ , where  $Z$  = cation charge,  $r$  = cation radius in Å) [49]. Based on the structural spectra study of the glasses, it can be concluded that barium and magnesium prefer the role of network modifiers. In the case of the AlF<sub>3</sub>, the aluminum acts as a glass network (in the coordination of four), as well as a network modifier ( coordinations of five and six) in the network of the BGG0.5Er glass. In each of the glass networks, the presence of the Ge(2), and Ge(3) units was confirmed. Due to magnesium's field strength, which is higher than the rest of the cations, Mg<sup>2+</sup> prefers to associate with more Ge(2) units than aluminum and barium. According to a crystal-chemistry approach based on a modified random network model, a depolymerized glass network increases the regularity of sites occupied by lanthanide ions [11]. The luminescence studies of erbium-doped glasses modified with fluoride compounds confirmed that the addition of fluorides leads to an enhancement in the NIR emission. The most intensive UC luminescence was observed in the sample with MgF<sub>2</sub> in both excitation schemes (808 and 980 nm).

#### 5. Conclusions

In this paper, a detailed analysis of the structural and luminescence properties of erbium-doped gallo-germanate glass modified by fluoride compounds (BaF<sub>2</sub>, MgF<sub>2</sub>, and AlF<sub>3</sub>) was performed. Based on the deconvoluted IR and Raman spectra, it was corroborated that the addition of the fluoride compounds into the BGG\_0.5Er glass resulted in a

decrease in its glass network polymerization. The decrease in the number of Ge(3) units at the expense of an increase in the Ge(2) units was found in the decomposed Raman spectra of each glass. The highest NBO/BO ratio was obtained for the BGG glass with the MgF<sub>2</sub>. In the glass network of the aluminum-modified BGG glass doped with Er<sup>3+</sup>, the presence of Al with different coordinations (tetra-, penta- and octahedral) was confirmed based on the <sup>27</sup>Al MAS NMR spectrum. For each glass, the most robust depolymerized network enhanced the regularity of the sites occupied by the erbium ions. The luminescence properties of the erbium ions in glasses were related to the results of the structural studies. In the case of visible emission, the green emission corresponding to the <sup>2</sup>H<sub>11/2</sub> and <sup>4</sup>S<sub>3/2</sub> levels was dominated in both of the used excitation channels. It is worth noticing that the luminescence profile depends on the fluoride modifiers employed and the excitation wavelength. Our experiment gives valuable information about luminescence behavior in relation to the structural modification of the host. In our further investigation, the next step will be the fabrication of transparent glass ceramics in the BGG0.5Er\_MgF<sub>2</sub> system. The BGG glass doped with erbium and modified by MgF<sub>2</sub> has better emission intensities and the lowest thermal stability of the other glasses.

**Author Contributions:** Conceptualization, M.L.; investigation, M.L., G.M., B.S., K.S., T.R., G.L.J., Z.O., M.K. (Marcin Kochanowicz), P.M., A.B., J.Ż. and M.K. (Marta Kuwik); data curation, M.L. and J.Ż.; writing—original draft preparation, M.L. and J.Ż.; writing—review and editing, D.D.; project administration, D.D.; funding acquisition, D.D.; formal analysis, J.P., W.P. and J.D. All authors have read and agreed to the published version of the manuscript.

**Funding:** The research activity was granted by the National Science Centre, Poland No. 2016/23/B/ST8/00706 and No. 2020/39/D/ST5/02287, as well as in part by the “Excellence Initiative—Research University” for the University of Science and Technology.

**Institutional Review Board Statement:** Not applicable.

**Informed Consent Statement:** Not applicable.

**Data Availability Statement:** Not applicable.

**Conflicts of Interest:** The authors declare no conflict of interest.

## References

1. McKeown, D.M.; Merzbacher, C.I. Raman Spectroscopic Studies of BaO–Ga<sub>2</sub>O<sub>3</sub>–GeO<sub>2</sub> Glasses. *J. Non-Cryst. Solids* **1995**, *183*, 61–72. [[CrossRef](#)]
2. Skopak, T.; Calzavara, F.; Ledemi, Y.; Célerié, F.; Allix, M.; Véron, E.; Dussauze, M.; Cardinal, T.; Fargin, E.; Messaddeq, Y. Properties, Structure and Crystallization Study of Germano-Gallate Glasses in the Ga<sub>2</sub>O<sub>3</sub>–GeO<sub>2</sub>–BaO–K<sub>2</sub>O System. *J. Non-Cryst. Solids* **2019**, *514*, 98–107. [[CrossRef](#)]
3. Calzavara, F.; Allix, M.; Dussauze, M.; Jubera, V.; Nalin, M.; Cardinal, T.; Fargin, E. Glass Forming Regions, Structure and Properties of Lanthanum Barium Germanate and Gallate Glasses. *J. Non-Cryst. Solids* **2021**, *571*, 121064. [[CrossRef](#)]
4. Jewell, J.M.; Higby, P.L.; Aggarwal, I.D. Properties of BaO–R<sub>2</sub>O<sub>3</sub>–Ga<sub>2</sub>O<sub>3</sub>–GeO<sub>2</sub> (R = Y, Al, La, and Gd) Glasses. *J. Am. Ceram. Soc.* **1994**, *77*, 697–700. [[CrossRef](#)]
5. Guérineau, T.; Strutynski, C.; Skopak, T.; Morency, S.; Hanafi, A.; Calzavara, F.; Ledemi, Y.; Danto, S.; Cardinal, T.; Messaddeq, Y.; et al. Extended Germano-Gallate Fiber Drawing Domain: From Germanates to Gallates Optical Fibers. *Opt. Mater. Express* **2019**, *9*, 2437. [[CrossRef](#)]
6. Hongisto, M.; Veber, A.; Petit, Y.; Cardinal, T.; Danto, S.; Jubera, V.; Petit, L. Radiation-Induced Defects and Effects in Germanate and Tellurite Glasses. *Materials* **2020**, *13*, 3846. [[CrossRef](#)]
7. Bérubé, J.-P.; Le Camus, A.; Messaddeq, S.H.; Petit, Y.; Messaddeq, Y.; Canioni, L.; Vallée, R. Femtosecond Laser Direct Inscription of Mid-IR Transmitting Waveguides in BGG Glasses. *Opt. Mater. Express* **2017**, *7*, 3124. [[CrossRef](#)]
8. Le Camus, A.; Petit, Y.; Bérubé, J.-P.; Bellec, M.; Canioni, L.; Vallée, R. Direct-Laser-Written Integrated Mid-IR Directional Couplers in a BGG Glass. *Opt. Express* **2021**, *29*, 8531. [[CrossRef](#)]
9. Kochanowicz, M.; Zmojda, J.; Miluski, P.; Baranowska, A.; Leich, M.; Schwuchow, A.; Jäger, M.; Kuwik, M.; Pisarska, J.; Pisarski, W.A.; et al. Tm<sup>3+</sup>/Ho<sup>3+</sup> Co-Doped Germanate Glass and Double-Clad Optical Fiber for Broadband Emission and Lasing above 2 μm. *Opt. Mater. Express* **2019**, *9*, 1450. [[CrossRef](#)]
10. Pisarska, J.; Kuwik, M.; Pisarski, W.A. Spectroscopic Properties of Inorganic Glasses Doped with Pr<sup>3+</sup>: A Comparative Study. *Materials* **2022**, *15*, 767. [[CrossRef](#)]

11. Żur, L.; Janek, J.; Sołtys, M.; Goryczka, T.; Pisarska, J.; Pisarski, W.A. Structural and Optical Investigations of Rare Earth Doped Lead-Free Germanate Glasses Modified by MO and MF<sub>2</sub> (M = Ca, Sr, Ba). *J. Non-Cryst. Solids* **2016**, *431*, 145–149. [[CrossRef](#)]
12. Fan, J.; Tang, B.; Wu, D.; Fan, Y.; Li, R.; Li, J.; Chen, D.; Calveza, L.; Zhang, X.; Zhang, L. Dependence of Fluorescence Properties on Substitution of BaF<sub>2</sub> for BaO in Barium Gallo-Germanate Glass. *J. Non-Cryst. Solids* **2011**, *357*, 1106–1109. [[CrossRef](#)]
13. Strutynski, C.; Calzavara, F.; Guerineau, T.; Loi, L.; Laberdesque, R.; Rampnoux, J.-M.; Morency, S.; Ledemi, Y.; Petit, Y.; Dussauze, M.; et al. Heavy-Oxide Glasses with Superior Mechanical Assets for Nonlinear Fiber Applications in the Mid-Infrared. *Opt. Mater. Express* **2021**, *11*, 1420. [[CrossRef](#)]
14. Marcondes, L.M.; Evangelista, R.O.; Gonçalves, R.R.; de Camargo, A.S.S.; Manzani, D.; Nalin, M.; Cassanjes, F.C.; Poirier, G.Y. Er<sup>3+</sup>-Doped Niobium Alkali Germanate Glasses and Glass-Ceramics: NIR and Visible Luminescence Properties. *J. Non-Cryst. Solids* **2019**, *521*, 119492. [[CrossRef](#)]
15. Rybaltovsky, A.A.; Sverchkov, S.E.; Vel'miskin, V.V.; Przhiiialkovskii, D.V.; Bazakutsa, A.P.; Galagan, B.I.; Denker, B.I.; Butov, O.V. Single-Frequency Continuous-Wave Laser Based on the Novel Er/Yb-Doped Composite Phosphosilicate Fiber. *Opt. Laser Technol.* **2022**, *151*, 108049. [[CrossRef](#)]
16. Wu, T.; Tong, R.; Liao, L.; Huang, L.; Zhao, S.; Xu, S. A Point Temperature Sensor Based on Upconversion Emission in Er<sup>3+</sup>/Yb<sup>3+</sup> Codoped Tellurite-Zinc-Niobium Glass. *Sensors* **2017**, *17*, 1253. [[CrossRef](#)] [[PubMed](#)]
17. Nanda, K.; Kundu, R.S.; Punia, R.; Mohan, D.; Kishore, N. Resonant and Non-Resonant Nonlinear Optical Properties of Er<sup>3+</sup> Modified BaO-ZnO-B<sub>2</sub>O<sub>3</sub> Glasses at 532 and 1550 Nm. *J. Non-Cryst. Solids* **2020**, *541*, 1201555. [[CrossRef](#)]
18. Marcondes, L.M.; Ramos da Cunha, C.; de Pietro, G.M.; Manzani, D.; Gonçalves, R.R.; Batista, G.; Cassanjes, F.C.; Poirier, G. Multicolor Tunable and NIR Broadband Emission from Rare-Earth-Codoped Tantalum Germanate Glasses and Nanostructured Glass-Ceramics. *J. Lumin.* **2021**, *239*, 118357. [[CrossRef](#)]
19. Quimby, R.S.; Miniscalco, W.J.; Thompson, B. Clustering in Erbium-doped Silica Glass Fibers Analyzed Using 980 Nm Excited-state Absorption. *J. Appl. Phys.* **1994**, *76*, 4472–4478. [[CrossRef](#)]
20. Yang, G.F.; Zhang, Q.Y.; Li, T.; Shi, D.M.; Jiang, Z.H. Laser-Diode-Excited Intense Luminescence and Green-Upconversion in Erbium-Doped Bismuth-Germanate-Lead Glasses. *Spectrochim. Acta Part A Mol. Biomol. Spectrosc.* **2008**, *69*, 41–48. [[CrossRef](#)] [[PubMed](#)]
21. Tanabe, S. Optical Properties and Local Structure of Rare-Earth-Doped Amplifier for Broadband Telecommunication. *J. Alloys Compd.* **2006**, *408–412*, 675–679. [[CrossRef](#)]
22. Pisarski, W.A.; Pisarska, J.; Dorosz, D.; Dorosz, J. Towards Lead-Free Oxyfluoride Germanate Glasses Singly Doped with Er<sup>3+</sup> for Long-Lived near-Infrared Luminescence. *Mater. Chem. Phys.* **2014**, *148*, 485–489. [[CrossRef](#)]
23. Taherunnisa, S.; Reddy, D.V.K.; SambasivaRao, T.; Rudramamba, K.S.; Zhydachevskyy, Y.A.; Suchocki, A.; Piasecki, M.; Reddy, M.R. Effect of Up-Conversion Luminescence in Er<sup>3+</sup> Doped Phosphate Glasses for Developing Erbium-Doped Fibre Amplifiers (EDFA) and G-LED's. *Opt. Mater. X* **2019**, *3*, 100034. [[CrossRef](#)]
24. Jimenez, G.L.; Shrestha, B.; Porter, T.; Starzyk, B.; Lesniak, M.; Kuwik, M.; Kochanowicz, M.; Szumera, M.; Lisiecki, R.; Dorosz, D. Highly efficient up-conversion green emission functionalized with a biocompatible polymer. *RSC Adv.* **2022**, *12*, 20074. [[CrossRef](#)]
25. Xu, S.; Yang, Z.; Dai, S.; Wang, G.; Hu, L.; Jiang, Z. Upconversion Fluorescence Spectroscopy of Er<sup>3+</sup>-Doped Lead Oxyfluoride Germanate Glass. *Mater. Lett.* **2004**, *58*, 1026–1029. [[CrossRef](#)]
26. Aktas, B.; Albaskara, M.; Dogru, K.; Yalcin, S. Mechanical Properties of Soda-Lime-Silica Glasses Doped with Eggshell Powder. *Acta Phys. Pol. A* **2017**, *132*, 436–438. [[CrossRef](#)]
27. Cai, M.; Wei, T.; Zhou, B.; Tian, Y.; Zhou, J.; Xu, S.; Zhang, J. Analysis of Energy Transfer Process Based Emission Spectra of Erbium Doped Germanate Glasses for Mid-Infrared Laser Materials. *J. Alloys Compd.* **2015**, *626*, 165–172. [[CrossRef](#)]
28. Zhou, L.; Huang, F.; Ren, G.; Hua, Y.; Lei, R.; Xu, S. Efficient Er<sup>3+</sup>: 4I11/2 → 4I13/2 Radiative Transition Regulated by Optimizing the Sensitization Mechanism. *Spectrochim. Acta Part A Mol. Biomol. Spectrosc.* **2020**, *228*, 117853. [[CrossRef](#)]
29. Shi-Qing, X.; Da-Wei, F.; Zai-Xuan, Z.; Shi-Long, Z.; Li-Yan, Z.; Bao-Ling, W.; Zhong-Hong, J. Host Dependent Thermal Stability and Frequency Upconversion of Er<sup>3+</sup>-Doped Heavy Metal Oxyfluoride Germanate Glasses. *Chin. Phys.* **2005**, *14*, 2246–2250. [[CrossRef](#)]
30. Bradtmüller, H.; Rodrigues, A.C.M.; Eckert, H. Network Former Mixing (NFM) Effects in Alkali Germanotellurite Glasses. *J. Alloys Compd.* **2021**, *873*, 159835. [[CrossRef](#)]
31. Skopak, T.; Hee, P.; Ledemi, Y.; Dussauze, M.; Kroeker, S.; Cardinal, T.; Fargin, E.; Messaddeq, Y. Mixture Experimental Design Applied to Gallium-Rich GaO<sub>3</sub>/2-GeO<sub>2</sub>-NaO<sub>1</sub>/2 Glasses. *J. Non-Cryst. Solids* **2017**, *455*, 83–89. [[CrossRef](#)]
32. Zhang, L.Y.; Li, H.; Hu, L.L. Statistical Structure Analysis of GeO<sub>2</sub> Modified Y<sup>3+</sup>: Phosphate Glasses Based on Raman and FTIR Study. *J. Alloys Compd.* **2017**, *698*, 103–113. [[CrossRef](#)]
33. Skopak, T.; Kroeker, S.; Levin, K.; Dussauze, M.; Méreau, R.; Ledemi, Y.; Cardinal, T.; Fargin, E.; Messaddeq, Y. Structure and Properties of Gallium-Rich Sodium Germano-Gallate Glasses. *J. Phys. Chem. C* **2019**, *123*, 1370–1378. [[CrossRef](#)]
34. Alvarado-Rivera, J.; Rodríguez-Carvajal, D.A.; Acosta-Enríquez, M.D.; Manzanares-Martínez, M.B.; Álvarez, E.; Lozada-Morales, R.; Díaz, G.C.; de Leon, A.; Zayas, M.E. Effect of CeO<sub>2</sub> on the Glass Structure of Sodium Germanate Glasses. *J. Am. Ceram. Soc.* **2014**, *97*, 3494–3500. [[CrossRef](#)]
35. Rachkovskaya, G.E.; Zakharevich, G.B. IR Spectra of Tellurium Germanate Glasses and Their Structure. *J. Appl. Spectrosc.* **2007**, *74*, 86–89. [[CrossRef](#)]

36. Lesniak, M.; Zeid, J.; Starzyk, B.; Kochanowicz, M.; Kuwik, M.; Zmojda, J.; Miluski, P.; Baranowska, A.; Dorosz, J.; Pisarski, W.; et al. Investigation of the TeO<sub>2</sub>/GeO<sub>2</sub> Ratio on the Spectroscopic Properties of Eu<sup>3+</sup>-Doped Oxide Glasses for Optical Fiber Application. *Materials* **2021**, *15*, 117. [[CrossRef](#)] [[PubMed](#)]
37. Yoshimoto, K.; Masuno, A.; Ueda, M.; Inoue, H.; Yamamoto, H.; Kawashima, T. Low Phonon Energies and Wideband Optical Windows of La<sub>2</sub>O<sub>3</sub>-Ga<sub>2</sub>O<sub>3</sub> Glasses Prepared Using an Aerodynamic Levitation Technique. *Sci. Rep.* **2017**, *7*, 45600. [[CrossRef](#)]
38. Szal, R.; Zmojda, J.; Kochanowicz, M.; Miluski, P.; Dorosz, J.; Lesniak, M.; Jeleń, P.; Starzyk, B.; Sitarz, M.; Kuwik, M.; et al. Spectroscopic Properties of Antimony Modified Germanate Glass Doped with Eu<sup>3+</sup> Ions. *Ceram. Int.* **2019**, *45*, 24811–24817. [[CrossRef](#)]
39. Chen, F.; Xu, S.; Wei, T.; Wang, F.; Cai, M.; Tian, Y.; Xu, S. Mid-Infrared Emission and Raman Spectra Analysis of Er<sup>3+</sup>-Doped Oxyfluorotellurite Glasses. *Appl. Opt.* **2015**, *54*, 3345. [[CrossRef](#)] [[PubMed](#)]
40. Koroleva, O.N.; Shtenberg, M.V.; Ivanova, T.N. The Structure of Potassium Germanate Glasses as Revealed by Raman and IR Spectroscopy. *J. Non-Cryst. Solids* **2019**, *510*, 143–150. [[CrossRef](#)]
41. Lotarev, S.V.; Lipatiev, A.S.; Lipateva, T.O.; Lopatina, E.V.; Sigaev, V.N. Ultrafast Laser-Induced Crystallization of Lead Germanate Glass. *Crystals* **2021**, *11*, 193. [[CrossRef](#)]
42. Carvalho, E.A.; Freitas, A.M.; Silva, G.H.; Bell, M.J.V.; Kassab, L.R.P.; Anjos, V. Thermal and Structural Analysis of Germanate Glass and Thin Films Co-Doped with Silver Nanoparticles and Rare Earth Ions with Insights from Visible and Raman Spectroscopy. *Vib. Spectrosc.* **2016**, *87*, 143–148. [[CrossRef](#)]
43. Wu, J.; Stebbins, J.F. Temperature and Modifier Cation Field Strength Effects on Aluminoborosilicate Glass Network Structure. *J. Non-Cryst. Solids* **2013**, *362*, 73–81. [[CrossRef](#)]
44. Lin, H.; Liu, K.; Pun, E.Y.B.; Ma, T.C.; Peng, X.; An, Q.D.; Yu, J.Y.; Jiang, S.B. Infrared and Visible Fluorescence in Er<sup>3+</sup>-Doped Gallium Tellurite Glasses. *Chem. Phys. Lett.* **2004**, *398*, 146–150. [[CrossRef](#)]
45. Żur, L.; Janek, J.; Sołtys, M.; Pisarska, J.; Pisarski, W.A. Effect of BaF<sub>2</sub> Content on Luminescence of Rare-Earth Ions in Borate and Germanate Glasses. *J. Am. Ceram. Soc.* **2016**, *99*, 2009–2016. [[CrossRef](#)]
46. Janek, J.; Lisiecki, R.; Ryba-Romanowski, W.; Pisarska, J.; Pisarski, W.A. Up-Conversion Luminescence of Er<sup>3+</sup> Ions in Lead-Free Germanate Glasses under 800 Nm and 980 Nm Cw Diode Laser Excitation. *Opt. Mater.* **2017**, *74*, 105–108. [[CrossRef](#)]
47. Cao, G.; Lin, F.; Hu, H.; Gan, F. A New Fluorogermanate Glass. *J. Non-Cryst. Solids* **2003**, *326–327*, 170–176. [[CrossRef](#)]
48. Zhao, Z.; Ai, B.; Liu, C.; Yin, Q.; Xia, M.; Zhao, X.; Jiang, Y. Er<sup>3+</sup> Ions-Doped Germano-Gallate Oxyfluoride Glass-Ceramics Containing BaF<sub>2</sub> Nanocrystals. *J. Am. Ceram. Soc.* **2015**, *98*, 2117–2121. [[CrossRef](#)]
49. Sreenivasan, H.; Kinnunen, P.; Adesanya, E.; Patanen, M.; Kantola, A.M.; Telkki, V.-V.; Huttula, M.; Cao, W.; Provis, J.L.; Illikainen, M. Field Strength of Network-Modifying Cation Dictates the Structure of (Na-Mg) Aluminosilicate Glasses. *Front. Mater.* **2020**, *7*, 267. [[CrossRef](#)]